THERMAL CONTROL OF CERAMIC BREEDER BLANKETS

A. RENÉ RAFFRAY, MARK S. TILLACK, and MOHAMED A. ABDOU
University of California–Los Angeles
Mechanical, Aerospace and Nuclear Engineering Department
Los Angeles, California 90024-1597

BLANKET ENGINEERING

KEYWORDS: *ceramic breeder blanket, thermal control, packed bed*

Received April 6, 1992
Accepted for Publication July 24, 1992

Thermal control is an important issue for ceramic breeder blankets since the breeder needs to operate within its temperature window for the tritium release and inventory to be acceptable. A thermal control region is applicable not only to situations where the coolant can be run at low temperature, such as for the International Thermonuclear Experimental Reactor (ITER) base blanket, but also to ITER test module and power reactor situations, where it would allow for ceramic breeder operation over a wide range of power densities in space and time. Four thermal control mechanisms applicable to ceramic breeder blanket designs are described: a helium gap, a beryllium sintered block region, a beryllium sintered block region with a metallic felt at the beryllium-cladding interface, and a beryllium packed-bed region. Key advantages and issues associated with each of these mechanisms are discussed. Experimental and modeling studies focusing on beryllium packed-bed thermal conductivity and wall conductance, and beryllium sintered block–stainless steel cladding contact resistance are then described. Finally, an assessment of the potential of the different mechanisms for both passive and active control is carried out based on example calculations for a given set of ITER-like conditions.

I. INTRODUCTION

Ceramic breeders need to operate within an allowable temperature window for the breeder tritium release and inventory to be acceptable. Thus, the thermal performance of ceramic breeder blankets is determined in large part by the predictability and controllability of the series of thermal resistances, including regions and interfaces, between the coolant and the ceramic breeder. Ideally, if the coolant temperature is high enough and the ceramic breeder temperature window is wide enough, the breeder can be separated from the coolant by a cladding only and still operate above its minimum allowable temperature, thereby minimizing the number of interface resistances and the associated uncertainties during operation. However, if operating conditions require a thermal disconnect between the ceramic breeder and the coolant, a thermal control region needs to be provided between the high-temperature ceramic breeder and the lower temperature coolant, as shown in Fig. 1.

This is particularly important when power production is not an objective, such as for the International Thermonuclear Experimental Reactor (ITER) base blanket; the coolant can then be kept at low temperature and pressure to enhance reliability and safety while the thermal control region enables ceramic breeder operation at high temperature for acceptable tritium release. A thermal control region would also apply for both the ITER test module and the power reactor situations to allow for operation at different power levels if the coolant temperature at the inlet to the breeder region is lower than the allowable ceramic breeder temperature. For ITER ceramic breeder test module application, a thermal control region would enable the ceramic breeder to operate within its temperature window over

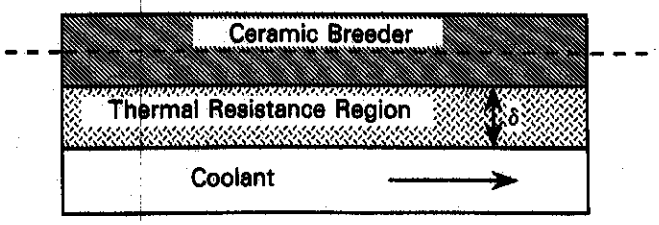

Fig. 1. Schema of thermal resistance region between high-temperature ceramic breeder region and low-temperature water coolant.

In addition, the temperature drops across the stainless steel claddings were assumed to be negligible compared with the overall temperature drop between the ceramic breeder and coolant.

Additional assumptions specific to each configuration are described in the following sections. Note that although the absolute controllability of different blanket concepts would change for different assumptions, such as power densities and coolant temperature, it is believed that the relative assessment of the performance of the different thermal control mechanisms provided by these example calculations would still apply.

V.A. Helium Gap

The helium thermal conductivity k_{He} is proportional to the temperature T to the power of ~0.72, according to the following correlation derived from results reported in Ref. 25:

$$k_{He} \sim 2.5 \times 10^{-3} T^{0.72} , \quad (13)$$

where k_{He} is in W/m·K and T is in kelvins.

This is an attractive characteristic of helium since it results in an extension of the range of allowable power variation. Typically, as the power is increased, the temperature drop across the helium gap increases, but because of the enhanced helium thermal conductivity, the increase is not in direct proportion to the power increase. Similarly, for a power decrease, the helium thermal conductivity decreases, and the resulting decrease in the helium temperature drop is not in direct proportion with the power decrease. Both these effects keep the ceramic breeder temperature within its allowable window over larger power increases and decreases, thus providing more flexibility in accommodating power variation. These effects were included in the thermal control calculations for the allowable wall load range as a function of the helium region thickness.

The calculation of allowable wall load range proceeded as follows. First, the temperature drop across each region was calculated for a P_N of 1.2 MW/m^2 and for the given assumptions. The maximum allowable P_N was then estimated as f_{max}, a multiple of 1.2 MW/m^2, based on the following equation:

$$f_{max}\{\Delta T_{f(0)} + [k_{He(0)}/k_{He(1)}]\Delta T_{He(0)} + \Delta T_{CB(0)}\} = T_{CB(max)} - T_{water} , \quad (14)$$

where the subscripts (0) and (1) refer to parameters calculated for the reference and final P_N values. The value of $k_{He(1)}$ can be estimated from the helium average temperature, $T_{He(1)}(ave)$, based on the variation of k_{He} with temperature. The term $T_{He(1)}(ave)$ is given by

$$T_{He(1)}(ave) = T_{water} + f_{max}\{0.5[k_{He(0)}/k_{He(1)}]\Delta T_{He(0)} + \Delta T_{f(0)}\} . \quad (15)$$

Equations (14) and (15) in conjunction with Eq. (13) were solved for the three unknowns, $k_{He(1)}$, $T_{He(1)}(ave)$, and f_{max}. Equation (14) was replaced by the following expression to calculate the minimum allowable P_N as f_{min}, a multiple of 1.2 MW/m^2:

$$f_{min}\{\Delta T_{f(0)} + [k_{He(0)}/k_{He(1)}]\Delta T_{He(0)}\} = T_{CB(min)} - T_{water} . \quad (16)$$

In addition, radiation can contribute significantly to the heat transfer, particularly for the high-temperature cases. Radiation is dependent on the emissivity of the surfaces, which is not known. As an upper bound, the effect of radiation was included based on the Stefan-Boltzmann law for a black surface.

The results are shown in Fig. 28 for cases with and without radiation. The allowable P_N range contracts rapidly as δ_{He} is decreased. In the absence of radiation, δ_{He} for a reasonable range of P_N (0.55 to 2 MW/m^2) is ~1.5 mm, which is small and gives rise to the concern of maintaining close tolerances during manufacture and operation. Radiation substantially increases the allowable upper wall load limit and would allow the choice of a larger gap size, depending on the emissivity of the surfaces. The effect is more marked for cases where the allowable wall load and corresponding heat flux are initially lower since the additional heat flux allowed by radiation for the same temperature drop across the gap is then relatively more important. Similarly, radiation also slightly increases the lower allowable wall load, but the effect is small since the temperatures involved are lower. For example, for a 3-mm gap thickness, the allowable wall range of 0.19 to 0.96 MW/m^2 excluding radiation is extended to a maximum of 0.32 to 2.32 MW/m^2 when including radiation. The actual range would be somewhere between

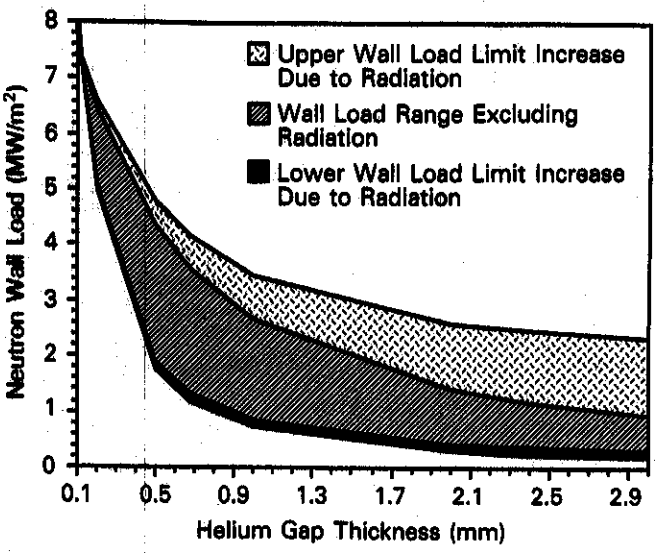

Fig. 28. Range of allowable wall loads based on the ceramic breeder temperature limits as a function of the helium gap thickness between the ceramic breeder and water coolant.

a range of power levels in space and time. In addition, the possibility of active control would allow for testing at different breeder temperature levels. For power reactors, a thermal control region would allow for operation at a fractional power level, consistent with utility operating modes, and for any ceramic breeder–coolant design combination requiring a temperature disconnect between the coolant and breeder.

Two types of thermal resistance regions proposed for the ITER base blanket[1] are (a) a thin helium gap and (b) a beryllium region that would perform both neutron multiplying and thermal barrier functions. The beryllium could be either in sintered block form or in packed-bed form. For the case of beryllium sintered blocks, which have a high thermal conductivity, it is conceivable that a feltlike material be inserted at the beryllium-cladding interface to increase the overall thermal resistance of the thermal control region and, thus, reduce the beryllium inventory if required.

Thermal control issues include the predictability of the thermal resistances, particularly during operation. For instance, in the case of the helium gap, uncertainties arise from the need to maintain close tolerances during manufacture and operation. In the case of the beryllium region, uncertainties are associated with the difficulty of predicting the effect of thermal expansion and irradiation swelling of beryllium on the thermal resistances of interfaces.

Besides predictability, other important features of an attractive blanket design are flexibility and robustness. These relate to the capability of the blanket to accommodate changes in parameters affecting the breeder temperature. These changes can be planned, as, for example, operation at different power levels. There could also be unpredictable changes in behavior caused, for instance, by the operating environment, such as effects of irradiation or thermal cycling. In addition, power level changes in space, as expected with tokamak reactors, and in time, if cyclic operation is used, have to be adequately accommodated.

The ability to actively control (*in situ*) the thermal resistance between the breeder and coolant would result in a more flexible and robust design and would alleviate some of the concerns associated with the uncertainty in the predictability of passive thermal control performance and in blanket operating conditions. Experimental and modeling studies were aimed at exploring mechanisms for active thermal control and at defining the limits of usefulness of these schemes. One such mechanism is the beryllium packed-bed region. Control of the effective thermal conductivity of the bed is obtained by changing the gas pressure and/or composition to vary the effective thermal conductivity of the bed. This behavior is also affected by the nature of the particle contact and by the size and surface characteristics of the particles. Experiments were conducted for both single-size and binary particle distributions under different gas pressures and flow rates.

In parallel with the experimental effort, modeling activities were carried out to develop tools for estimating the effective thermal conductivity of beryllium-helium packed beds as well as the contact resistance of beryllium sintered block–steel cladding interfaces. The models were used to help analyze experimental results as well as to assess their predictive capabilities over a range of experimental conditions.

In this paper, proposed thermal control schemes for ceramic breeder blankets are described, and key advantages and issues associated with each of them are discussed. Next, recent developments in modeling and experimental studies on beryllium thermal behavior are discussed. In light of these developments, an assessment of the potential of the thermal control mechanisms is carried out based on example calculations for a given set of ITER-like conditions.

II. THERMAL CONTROL CONFIGURATION

Two possible types of thermal resistance regions are a thin helium gap and a beryllium region. The beryllium can either be in sintered block form or packed-bed form. These configurations are described in the following, and the major advantages and issues associated with them are discussed.

II.A. Helium Gap

Use of a helium gap as a thermal barrier between the ceramic breeder and coolant is attractive based on the potential simplicity of the configuration and the ease of predictability of its thermal resistance provided the operating conditions and gap thickness are known. It has been used successfully in small-scale *in situ* tritium release experiment in fission reactors. However, for ITER-like power densities and even for the low-temperature coolant case, the gap thickness required to produce the necessary temperature drop between the coolant and breeder is small, and the resulting thermal resistance is sensitive to even small changes in the geometry. Thus, for large-scale blanket application, the key concerns remain the close tolerance required during manufacture and assembly as well as the ability to predict the gap dimensions during operation. These concerns are exacerbated if the blanket configuration requires variable gap thicknesses to account for poloidal power variation and bending of the blanket unit cell to accommodate space restriction or reactor contours, such as in the case of a poloidal blanket tube geometry.

II.B. Beryllium Region

The thermal resistance between the ceramic breeder and the coolant can also be provided by a beryllium region, which performs the dual function of neutron multiplying and thermal control. The beryllium can be either in sintered block form or in packed-bed form,

for which the advantages and issues are not necessarily the same. They are discussed separately in the following sections.

II.B.1. Beryllium Sintered Block

Use of a beryllium sintered block thermal control region is typified by the multilayered ceramic breeder blanket configuration proposed for the ITER base blanket[1,2] and shown in Fig. 2. It consists of layers of Li_2O breeder separated from the coolant by layers of beryllium in sintered block form, which provide the necessary thermal resistance between the breeder and the water coolant. Uncertainties in the thermal control performance are mostly associated with the predictability of the beryllium-cladding interface contact resistance. Any geometry or contact characteristic changes during operation could significantly affect the interface thermal resistance and, hence, the thermal control performance.

Beryllium in sintered block form has a high thermal conductivity and, depending on the heat generation in the ceramic breeder and the beryllium and on the required temperature drop between the coolant and the breeder, the beryllium region thickness can be quite high to provide the required temperature drop between the ceramic breeder and coolant. For this multilayer ceramic breeder blanket under ITER conditions, the beryllium region thickness varies from ~3 to 15 cm, depending on the radial and poloidal position of the blanket segment. This is advantageous in terms of minimizing the number of ceramic breeder and multiplier regions and, hence, of coolant and purge channels in the blanket. However, it also results in the use of a large amount of beryllium, whose unit cost is high. In addition, the tritium breeding benefit gained from using beryllium as a neutron multiplier tends to saturate with a beryllium thickness within ~10 cm, depending on the blanket configuration.

Two possible ways of minimizing the use of beryllium in the blanket are to insert a metallic felt at the beryllium sintered block–cladding interfaces or to use a packed bed of beryllium, at least for the thicker beryllium block regions. However, thinner beryllium layers tend to increase the number of ceramic breeder and beryllium layers required for reasonable tritium breeding performance, and any resulting increase in design

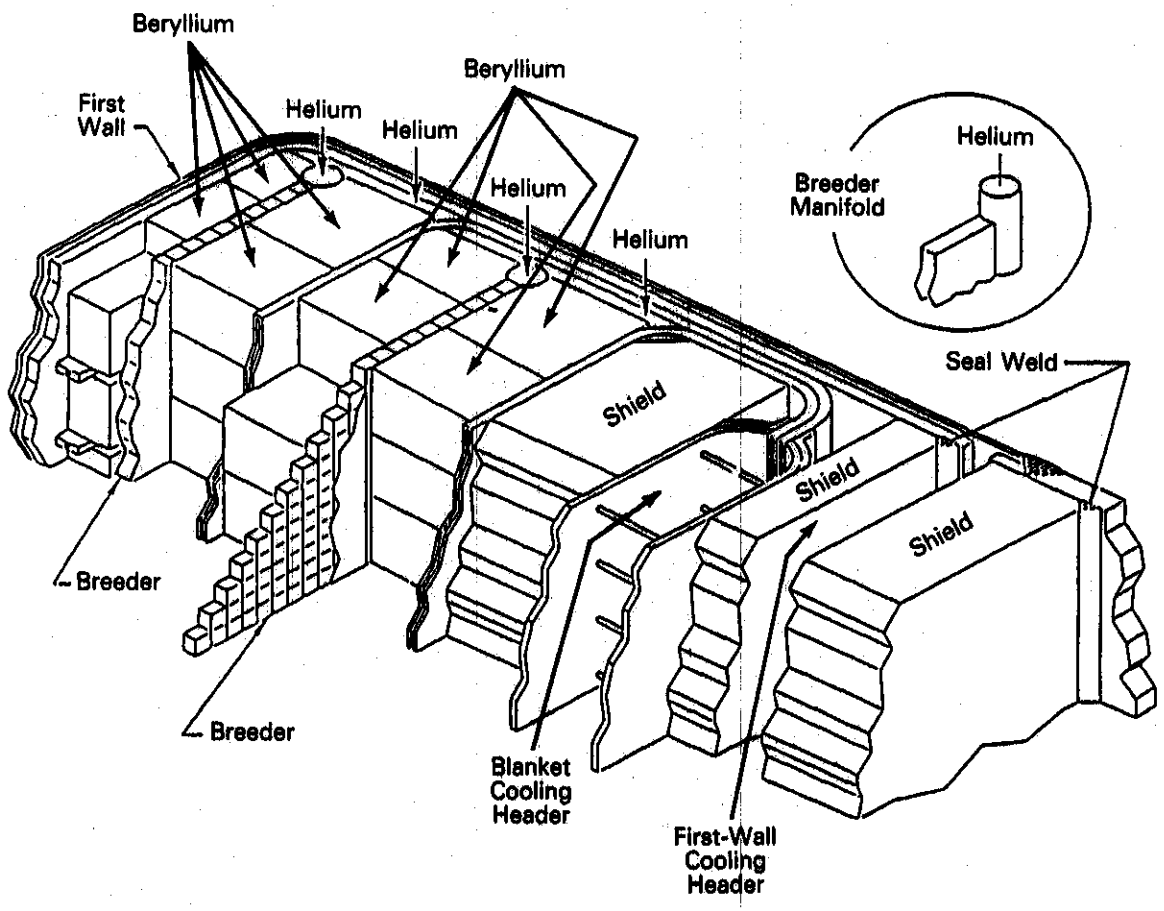

Fig. 2. Isometric view of multilayered ceramic breeder blanket design using a beryllium sintered block region for breeder thermal control.[1]

complexity must also be taken into account. These two alternative beryllium configurations are discussed in the next two sections.

II.B.2. Beryllium Sintered Block with Metallic Felt

Placing a metallic felt at the breeder interface was proposed in Ref. 3 to provide a reasonable degree of contact resistance predictability. Additionally, a metallic felt at the beryllium-cladding interface would provide the advantages of accommodation of beryllium swelling and thermal expansion through felt compressibility and the possibility of active thermal control through gas pressure adjustment.

Manufactured metallic felts are available with theoretical densities ranging from at least 10 to 60% and with fibers as small as 8 μm. Initial evaluation of the mechanical performance of the felt indicates that the felt does not serve any load-carrying functions and that the resulting stresses would be chiefly due to fiber bending under compression. They were estimated as being low based on a simple cantilever model. However, because of the irradiation environment, a number of concerns exist, including the effects of helium embrittlement, irradiation hardening, and radiation creep, which could cause the felt to disintegrate. Thus, the performance of the felt would need to be demonstrated under prototypical irradiation and temperature conditions.

II.B.3. Beryllium Packed Bed

An example of the use of a beryllium packed-bed thermal control region is shown in Fig. 3. It represents another multilayered ceramic breeder blanket configuration proposed for the ITER base blanket,[1] in which the Li_2O breeder is separated from the water coolant by a beryllium packed-bed region.

The packed-bed form offers the advantages of potential active control of the thermal conductance of the beryllium region through adjustment of the gas pressure or composition and possibly better accommodation of beryllium thermal expansion and swelling. It also makes minimum use of beryllium since the lower thermal conductivity of the packed bed results in thinner beryllium layers as compared with the sintered block form. However, this may lead to a larger number of layers and, thus, to a more complex design, as dictated by the neutronics for optimum tritium breeding. Other concerns relate to the predictability of the wall conductance during operation, to the effect of swelling or thermal expansion on the effective thermal conductivity of the bed, and to the bed behavior under cyclic conditions.

III. EXPERIMENTAL STUDIES

Because of the importance of thermal control for ceramic breeder blankets—in particular for ITER

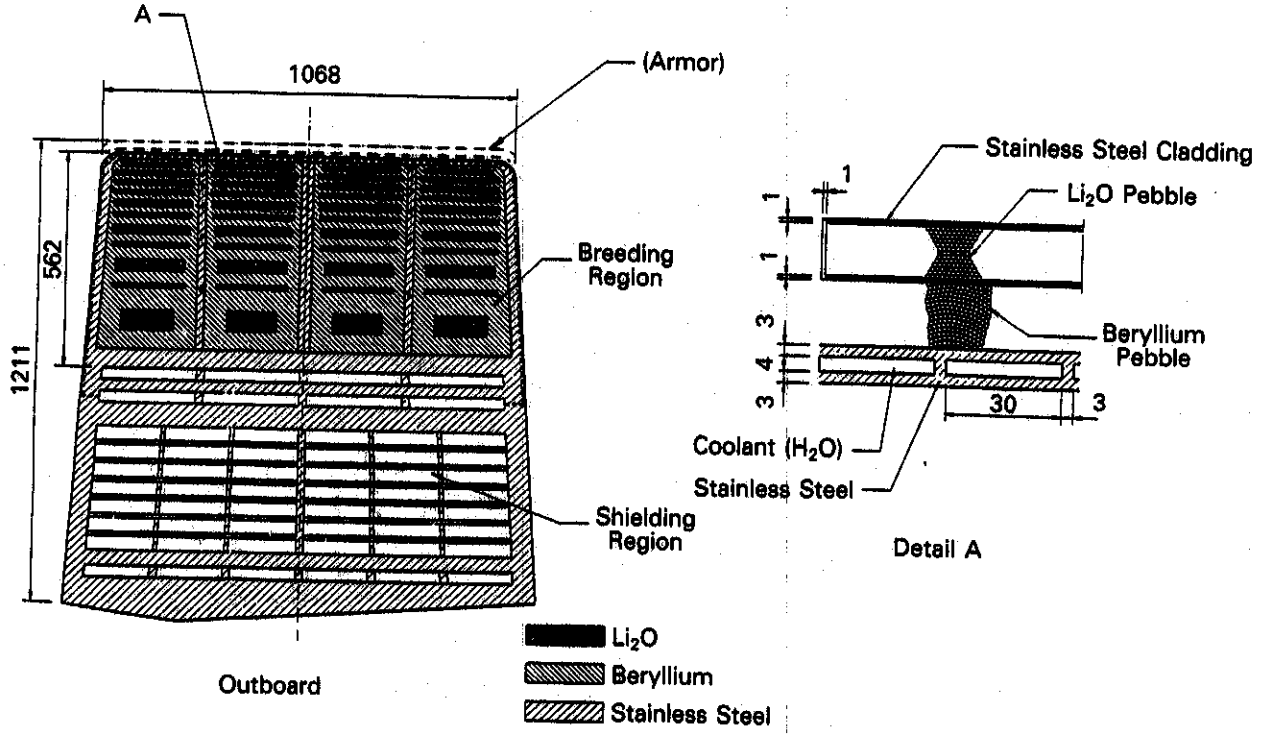

Fig. 3. Cross-sectional view of multilayered ceramic breeder blanket design using a beryllium packed-bed region for breeder thermal control.[1] Dimensions are given in millimetres.

application—a program of model development and experimentation has been undertaken to address key issues associated with the proposed thermal control mechanisms.

The effort initially focused on experimental and modeling studies of particle beds because of their unique thermal-hydraulic properties. The objective of the experimental program was to determine the effective thermal conductivity of a packed bed with a high ratio of solid to gas conductivity (to simulate beryllium-helium beds) and to ascertain the potential of active control of the effective thermal conductivity by variation of the gas pressure or composition. In parallel with the experimental effort, models were developed to help interpret the experimental data and to enable extrapolation to different reactor conditions. The experimental effort is covered in this section and the modeling effort in Sec. IV.

Experiments were conducted for both single-size and binary particle distributions under different gas pressures and flow rates.[4,5] Aluminum was chosen to simulate the physical properties of beryllium, which is the material proposed for reactor applications. Helium and nitrogen were used for the gas component. A cross section of the test section is shown in Fig. 4. Axial thermocouple penetrations were found to least affect the heat transfer characteristics of the bed and were used for all measurements. The axially inserted thermocouples were placed at five different radial positions to provide enough data to derive the radial temperature gradient and to estimate the corresponding effective thermal conductivity of the bed. Thermocouples were also placed at the inner cladding to evaluate the wall conductance. Thermocouples were not provided at the outer cladding because the temperature gradient there is generally too low to make an accurate determination of the wall conductance.

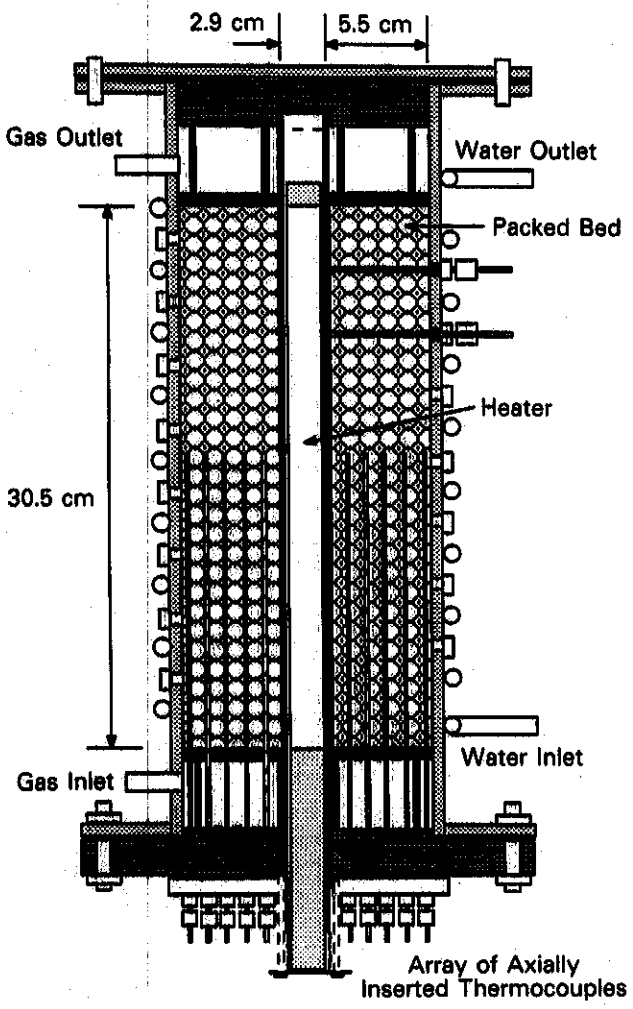

Fig. 4. Particle-bed test section.

III.A. Materials Forms and Test Matrix

Extensive data have been accumulated for the bulk thermal conductivity in aluminum beds with helium and N_2 gas constituents. Three particle sizes were studied, as described in Table I. In addition, binary beds were created using all combinations of the three sizes. The water coolant was run at room temperature for all cases to focus on lower temperature data (i.e., bed temperatures of ~50°C) where the effect of thermal radiation would be small.

All beds were packed and measured several times to establish the reproducibility of the data. Temperature profiles were measured in each bed for gas pressures ranging from ~0.005 to 3 atm. The packing procedure is very important in obtaining uniform tight packing. A vibratory table was used with success. In binary beds, a two-step procedure was used whereby the large fraction is packed first and then the smaller fraction is allowed to sift through the bed by vibration. The method is described more thoroughly in Ref. 4. Even with this careful procedure, a variation of several percent in average packing fraction was observed for beds of the same composition.

TABLE I

Particle Sizes and Packing Fractions Obtained

Bed Type	Particle Sizes	Packing Fraction Range (%)
Gas-atomized powder	75 to 150 μm	57 to 59
Centrifugally atomized shot	0.4 to 0.7 mm	60 to 64
Ball bearings	4.3 mm	62 to 65
Binary	4.3 + 0.5 mm	80 to 86
Binary	4.3 + 0.1 mm	83 to 87

III.B. Experimental Results

III.B.1. Thermal Conductivity

Assuming the bed is uniform, axisymmetric, and at steady state, the experimental value of the effective thermal conductivity is derived from the measurement of temperatures using the equation for the temperature profile in an annulus (see Nomenclature on p. 306):

$$k_{eff} = \frac{Q \log(r_o/r_i)}{2\pi L \Delta T_{bed}} , \quad (1)$$

where

Q = power to the heater

r_i, r_o = inner and outer radii of the bed

L = heated length

ΔT_{bed} = temperature difference across the bed.

The experimental accuracy of measurements of the effective thermal conductivity of a packed bed depends partly on the accuracy with which the relevant temperature difference, the input power, and the geometrical dimensions can be determined. Generally, errors in the measurement of these parameters resulted in an error of ~10% in the calculation of k_{eff}. Additional errors due to lack of axial uniformity, created, for example, by axial end losses, were minimized by making the temperature measurements at the axial midplane.

Results of several repetitive tests show good reproducibility of the data—within ±10%. Each time a new bed is packed, a slightly different packing fraction is obtained, which can have a substantial effect on the conductivity at higher pressures. Figures 5, 6, and 7

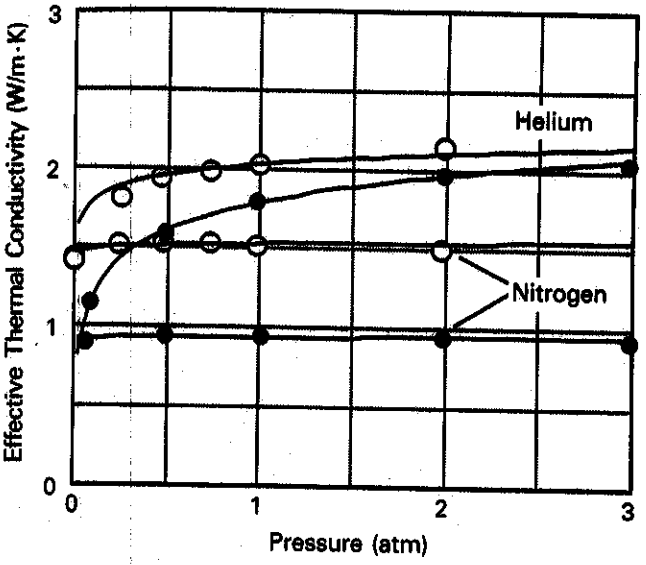

Fig. 6. Effective thermal conductivity of 0.5-mm aluminum packed beds with two different packing fractions and with helium and N_2 fill gas as a function of gas pressure. The open circles indicate a 62.4% packing fraction, and the solid circles indicate a 60.3% packing fraction.

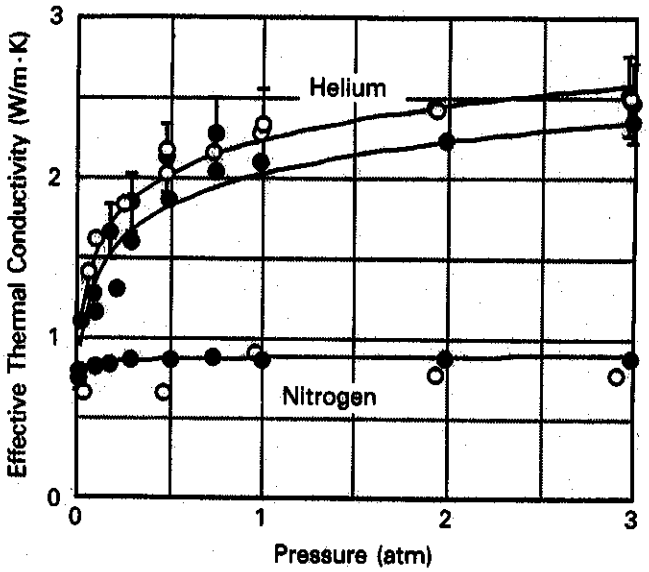

Fig. 5. Effective thermal conductivity of 4.3-mm aluminum packed beds with two different packing fractions and with helium and N_2 fill gas as a function of gas pressure. The open circles indicate a 65% packing fraction, and the solid circles indicate a 62.6% packing fraction.

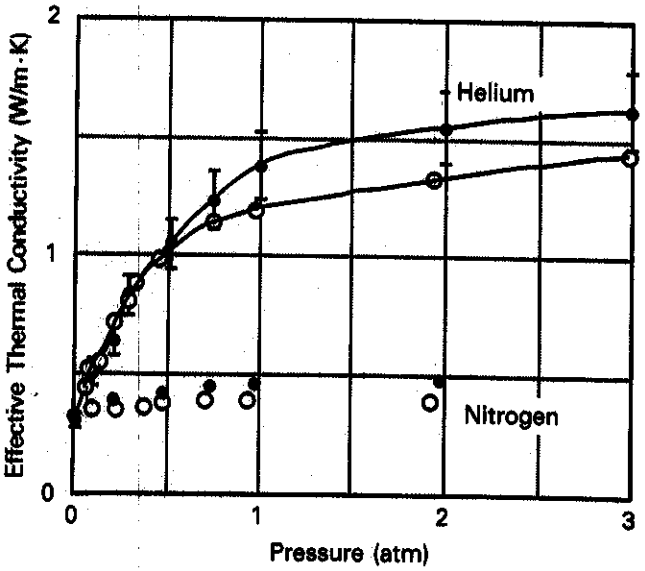

Fig. 7. Effective thermal conductivity of 0.1-mm aluminum packed beds with two different packing fractions and with helium and N_2 fill gas as a function of gas pressure. The open circles indicate a 57.4% packing fraction, and the solid circles indicate a 58.8% packing fraction.

show the effective thermal conductivity in 4.3-, 0.5-, and 0.1-mm single-size beds. The powder bed shows the largest variation of conductivity with pressure—a factor of 4 change from 0.1 to 3 atm. This is believed to be due to the poorer metal-to-metal contact resulting from surface roughness and irregular shapes, which leads to greater relative influence by the gas phase, as well as to the smaller characteristic length for gas conduction, which enhances the Smolukovski effect at the experimental gas pressure range. A change of 0.025 in the packing fraction changes the high-pressure conductivity by 10 to 15%. At very low pressure, the helium data tend to meet with the N_2 data, indicating that gas conduction is essentially eliminated, and heat is transferred through the solid contacts alone below ~0.1 atm.

The data for binary beds indicate a much stronger variation with packing fraction. There is a smaller percentage variation of thermal conductivity with pressure, as compared with the single-size beds having particle size the same as the smaller particles in the binary bed. The conductivity at 1 atm changes from 6 to 9.5 W/m·K as the packing fraction increases from 80 to 86%. As with single-size beds, the conductivity at low pressure tends to coincide with that of N_2, suggesting that solid contact conductance dominates in this regime. Figure 8 summarizes several data sets with a binary 0.5-mm + 4.3-mm bed and helium and N_2 fill gas. Figure 9 summarizes data with a binary 0.1-mm + 4.3-mm bed and helium fill gas only. Porosities are shown next to the curves.

Overall, the results tend to show lower k_{eff}/k_g values than results reported in Ref. 6 for single-size steel-

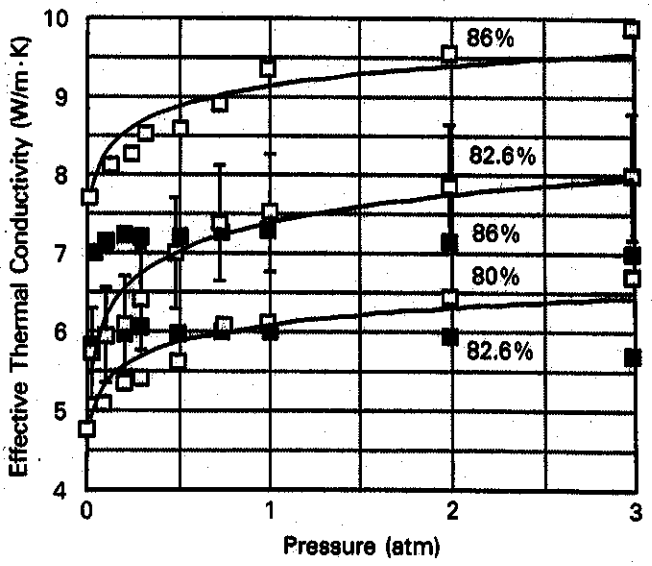

Fig. 8. Effective thermal conductivity of 4.3-mm + 0.5-mm aluminum binary packed beds with different packing fractions and with helium and N_2 fill gas as a function of gas pressure. The open squares denote helium, and the solid squares denote N_2.

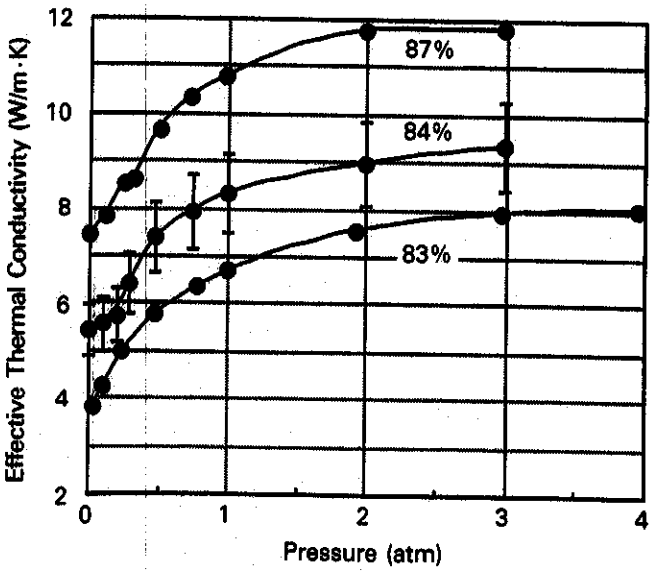

Fig. 9. Effective thermal conductivity of 4.3-mm + 0.1-mm aluminum binary packed beds with different packing fractions and with helium fill gas as a function of gas pressure.

air, zirconium-argon, and uranium-argon beds, which have lower solid thermal conductivities but about the same k_s/k_g ratio as aluminum-helium. For example, results for the k_{eff}/k_g ratio of 3.18-mm steel-air packed beds of porosity 0.4 are higher than the k_{eff}/k_g values shown in Fig. 5 for a 4.3-mm particle diameter and a porosity of 0.35 by ~33% at 1 atm and up to a factor of 2.3 at 0.1 atm. The k_{eff}/k_g results from Fig. 5 for the 4.3-mm particles are similar in terms of both magnitude and variation with pressure to those for single-size uranium-argon and zirconium-argon packed beds of porosity 0.4 but with 0.19-mm particles. Three runs from the experimental results reported in Ref. 7 involve 2-mm particle beds of aluminum and helium at 1 atm, of porosity 0.394. The effective thermal conductivity values from these runs are higher by a factor of ~2.5 to 3 than those shown in Fig. 5 for a helium pressure of 1 atm. It is believed that these disagreements are caused by such factors as the contact area, which depends on the packing technique and operating conditions; the surface roughness characteristics; and the effect of a finite oxide layer, all of which are particularly important for cases with high k_s/k_g ratios. The model described in Sec. IV.A includes the effect of the contact area and surface characteristics that are discussed there. There is a strong indication, however, that although the trends reported could be generalized, the magnitude of the effective thermal conductivity is very much dependent on the material characteristics, packing techniques, and operating conditions. For a blanket application, k_{eff} should be measured for the prototypical materials using prototypical packing techniques and operating conditions.

III.B.2. Wall Conductance

A small difference occurs between the measured temperature at the inner wall and the extrapolated temperature from the bed to the wall. This occurs primarily because the presence of a wall disturbs the local packing, resulting in higher local porosity and additional resistance to heat transfer.

The temperature jump at the inner and outer walls of the bed can be determined by extrapolating the bed internal temperatures to the wall using a linear regression fit of T against $\log(r)$. The extrapolated temperature is then compared with the measured temperature at the wall. The temperature difference is used to determine an effective wall conductance h_w:

$$q'' = h_w \Delta T_w \ , \qquad (2)$$

where

q'' = surface heat flux

ΔT_w = temperature difference between wall and bed extrapolation.

The relative effect of the wall region is expected to increase as the particle diameter increases because the size of the wall region increases with particle size. For 4.3-mm particles, the temperature jump was 10 to 15°C (with q'' ~3000 W/m^2), which is large enough to measure accurately. However, for single-size beds with 0.5- or 0.1-mm particles, the temperature jump at the wall is observed to be a small fraction of the temperature difference across the bed (<5 to 10%). In these cases, the actual value of the temperature jump is usually less than ~5°C, and the data have large uncertainties. We can only state that in these cases, the wall conductance is greater than ~1500 W/m^2·K.

Figure 10 shows data for the wall conductance in a single-size 4.3-mm bed with both helium and N_2 fill gas. A small increase in h_w is seen for helium as the pressure increases from near 0 to 1 atm (although the uncertainty is a large fraction of the total variation with pressure). The variation is only ~20%, in contrast with k_{eff}, which varies by a factor of 3. With N_2 fill gas, the variation with pressure is absent, and the absolute magnitude is only slightly lower than with helium fill gas. This suggests that for the assumed wall conductance definition, the contribution from the gas phase in the Smolukovski regime is small, even with helium.

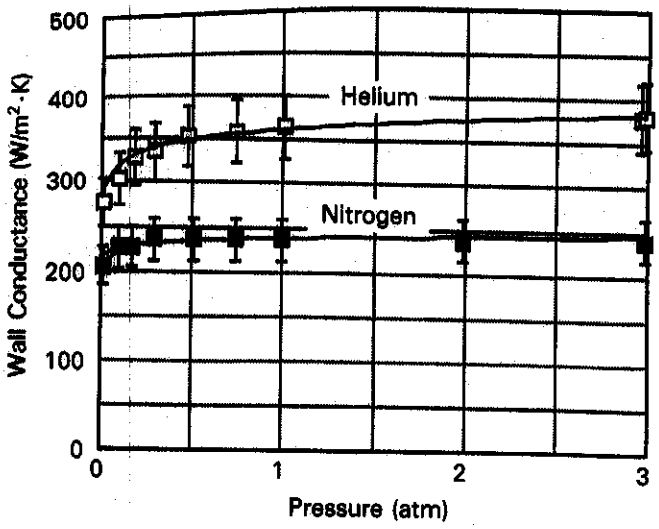

Fig. 10. Wall conductance at the inner annular wall of a 4.3-mm aluminum packed bed with helium and N_2 fill gas as a function of gas pressure.

Another case of interest is the binary beds, in which the bed conductivity is so large that the wall region can cause a significant relative temperature jump, even with smaller particles. The data are presented in tabular form (see Table II) since for these cases also, there is no measurable variation with pressure.

Binary beds have a higher packing fraction and a larger number of contact points, so that one expects less contribution from the gas phase. This seems to be borne out by the data. The helium and N_2 data are nearly identical for a given particle mixture and do not depend on pressure. The wall conductance for the 0.1-mm + 4.3-mm bed is substantially lower than for the 0.5-mm + 4.3-mm bed. This is consistent with the single-size thermal conductivity data (Figs. 5, 6, and 7), which indicates that the powder has much lower conductivity than the other two sizes in the regime dominated by metal-to-metal contact (i.e., with N_2 or low-pressure helium). The lower conductivity can be explained by the

TABLE II

Wall Conductance for Binary Beds with Helium and N_2 Fill Gas

Particle Sizes (mm)	Fill Gas	Packing Fraction (%)	h_w (W/m^2·K) (±10 to 20%)
4.3 + 0.5	Helium	86.1	880
4.3 + 0.5	N_2	86.1	870
4.3 + 0.1	Helium	87.1	550
4.3 + 0.1	N_2	87.1	540

different surface characteristics of the powder. The 100-μm gas-atomized powder has a very rough surface, irregular shape, and probably more oxide near the surface. The data also suggest that the binary wall conductance is dominated by the small-size fraction.

IV. MODELING STUDIES

The modeling effort primarily included development of models for the effective thermal conductivity of packed beds in support of the experimental effort. A simple model for estimating the lower limit of the wall conductance of a packed bed was also developed to provide a conservative estimate of the interface thermal resistance compared with the bulk thermal resistance for beds with high solid-to-gas conductivity ratios. Finally, modeling studies were carried out to address the beryllium sintered block–cladding interface resistance.

IV.A. Packed-Bed Effective Thermal Conductivity

To accurately model the thermal behavior of metallic packed beds, several key parameters must be included in the model, as follows:

1. *Sizes of particles:* The gas conductivity is markedly affected by pressure changes in the Knudsen (molecular) region. The local characteristic dimension determining the gas conduction regime (i.e., molecular, regular, or transition) varies in proportion to the particle size. It is expected that the effect of pressure changes on the effective thermal conductivity are more important for a packed bed with smaller particle sizes.

2. *Contact area between particles:* The contact area between particles plays an increasingly important role in determining the heat flow path as the solid-to-gas conductivity ratio, k_s/k_g, increases. The combination of the contact area, nature of the contact, and k_s/k_g value determines the fraction of the total heat transfer flowing through the contact. If this fraction is high, there is correspondingly only a small fraction of heat transferred through the gas, and any change in the gas thermal conductivity through pressure variation would have a small effect on the overall packed-bed effective thermal conductivity.

3. *Roughness characteristics:* Both the roughness height and density are important, particularly for characterizing the nature of the contact. Over the interfacial area, the roughness density determines the actual solid-to-solid contact with gas trapped between the roughnesses over a thickness determined by the roughness height.

4. *Binary size mixtures:* To achieve the packing fractions necessary for good breeding performance, a binary size distribution is necessary. Thus, the model should have the capability of accounting for both single-size and binary packing.

Note that since the experimental metallic packed bed of Refs. 4 and 5 was operated at a relatively low temperature and since the beryllium maximum temperature in a blanket is limited to ~500 to 600°C based on swelling considerations, radiation effects would tend to be relatively small (~5% or less) and would not need to be incorporated into the k_{eff} model.

Two possible modeling approaches are the deterministic and the statistical approaches. The deterministic approach assumes that the particle bed consists of a number of regular geometric configurations (or unit cells) and calculates k_{eff} based on that geometry. The statistical approach can be applied to random packed-bed configurations, and the influence of various microstructural formations is treated statistically.

Based on the relatively good agreement of available one-dimensional deterministic models (e.g., Refs. 8 and 9) with experimental data for different types of packed beds and on the ability of such models to account for gas pressure effects, a deterministic approach is chosen. For packed beds with a high k_s/k_g ratio, it is believed that the isotherms will be curved within the particles, particularly for cases with larger contact areas, which result in most of the heat flowing through the solids and contacts. To better account for the curvature of the isotherms, it is desirable that the model be at least two-dimensional, which would require a computational approach because of the complexity of the two-dimensional solution.

IV.A.1. Model Description

The two-dimensional model, described more fully in Refs. 10 and 11, is based on the one-dimensional approach of Ref. 12. It assumes that the packed-bed arrangement is essentially orthorhombic. Typically, a single-size packed bed has a porosity of 0.36 to 0.4, and the arrangement is ~80% orthorhombic (with a corresponding porosity of 0.395) on the average, with the rest probably being double nested, thus accounting for the lower porosities.[4,5,13]

A three-dimensional orthorhombic unit cell can be converted to a two-dimensional one, as shown in Fig. 11, by setting r_f so as to reproduce the desired porosity. To overcome the large temperature jump condition at the solid-gas interface, a spherical grid was used. The advantage of using a spherical grid is the ability to form a very fine mesh at the solid-gas interface and in the gas, where large temperature drops occur, and a coarse mesh in the solid, where temperatures do not vary as much. The following two-dimensional heat conduction equation in spherical coordinates was expressed in finite difference form and solved using a successive overrelaxation (SOR) scheme for given boundary conditions (adiabatic on each side of the unit cell due to symmetry and fixed temperatures T_1 and T_2

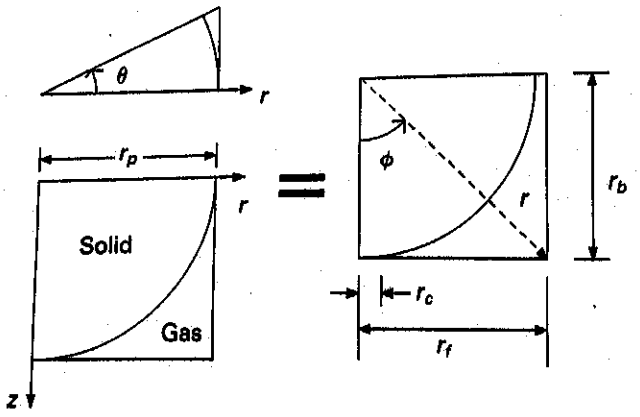

Fig. 11. Orthorhombic unit cell rearrangement from three-dimensional (r,θ,z) to two-dimensional (r,ϕ).

on the upper and lower boundary of the unit cell, respectively):

$$\frac{\partial}{\partial r}\left(kr^2\frac{\partial T}{\partial r}\right)+\frac{1}{\sin\phi}\frac{\partial}{\partial\phi}\left(k\sin\phi\frac{\partial T}{\partial\phi}\right)=0\ . \quad (3)$$

The thermal conductivity is specified at each node inside the grid. To account for pressure variation in the molecular regime, the gas conductivity was expressed as a function of an effective jump distance σ (Ref. 14):

$$k_g=\frac{k_{g(con)}}{(1+\sigma)}\ , \quad (4)$$

where $k_{g(con)}$ is the gas thermal conductivity in a continuum regime. The effective jump distance is based on the gas thermal accommodation coefficient α, ratio of specific heat γ, Prandtl number Pr, and mean free path λ (Ref. 14):

$$\sigma=4\frac{2-\alpha}{\alpha}\frac{\gamma}{\gamma+1}\frac{1}{\mathrm{Pr}}\frac{\lambda_{std}}{P}\frac{T}{273}\frac{1}{\delta_l}\ , \quad (5)$$

where

λ_{std} = gas mean free path at 273 K and 1 atm

P = pressure

δ_l = local characteristic length.

Once the temperature field is obtained for the unit cell, the local heat flow q_{uc} at the upper boundary is calculated from the local thermal conductivities and temperature gradients of the finite difference grid. Since the sides are adiabatic, the heat flux entering the unit cell at the upper boundary (at temperature T_2) must be the same as the heat flux leaving at the lower boundary (at temperature T_1). The effective thermal conductivity is then calculated from

$$k_{eff}=\frac{q_{uc}r_b}{A_{uc}(T_1-T_2)}\ , \quad (6)$$

where A_{uc} is the unit cell area.

IV.A.1.a. Surface Roughness. Previously developed models seldom account for these surface characteristics because of a lack of surface property data and difficulty in modeling. For the case of high k_s/k_g ratios, especially in the interfacial region (defined by r_c in Fig. 11), roughness effects on the heat transfer can be important. Roughness is incorporated in the model in a simple way based on Ref. 15. Basically, surface roughnesses are modeled as cylindrical elements of radius R_1 and height δ_r, with a density of one roughness per cylindrical surface unit area corresponding to a radius R_2, as illustrated in Fig. 12. Thus, in effect, actual contact occurs over a fraction $(R_1/R_2)^2$ of the interfacial area. The magnitudes of parameters R_1/R_2 and δ_r are estimated roughly from available particle surface examination data and are fine-tuned so as to best fit the experimental data.

IV.A.1.b. Binary Mixture. The modeling of a binary mixture is based on the progressive filling method of Ref. 12. In this case, the gas in Fig. 11 is replaced by the fine particle packing, and the solid circle represents one of the large spheres, as shown in Fig. 13. In the lower left corner of Fig. 13, there is a void space

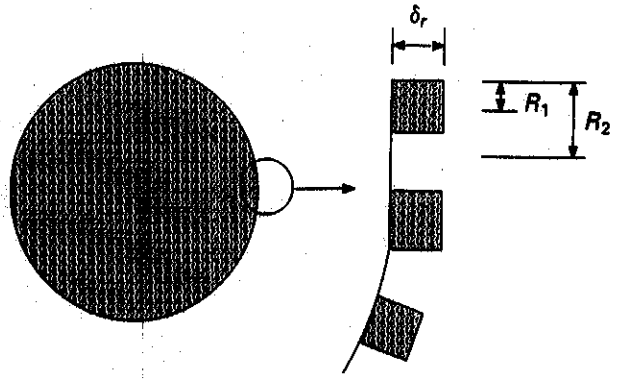

Fig. 12. Modeling of surface roughness.

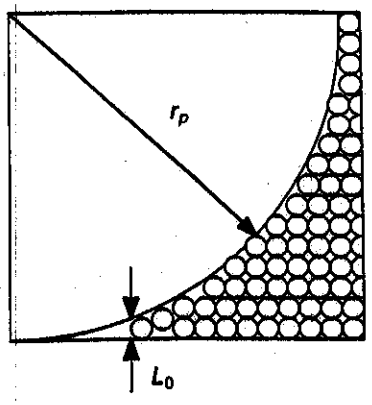

Fig. 13. Representation of binary mixture of spherical particles.

between the two large spheres where the smaller particles cannot fit. This void space is determined by the diameter of the fine particles. Thus, there are effectively three regions: the large sphere, which is pure solid; the void, which is pure gas; and the fine particle region, whose porosity is determined from the porosity of the single-large-particle bed, the binary bed porosity, and the void area. The calculation proceeds by first estimating k_{eff} for the fine single-size mixture and then using this k_{eff} (fine) to determine the overall k_{eff} for the three-region binary mixture unit cell. The model would then be applicable to binary beds with size ratios of ~7 or higher in which the fine mix could be considered to pack as a single-size bed within the space provided by the large spheres.

IV.A.1.c. Three-Dimensional Effect. To determine the effect of three-dimensional heat transfer, a fully three-dimensional orthorhombic unit cell, as shown on the left side of Fig. 11, was also modeled. The three-dimensional heat conduction equation in cylindrical coordinates was expressed in finite difference form and then solved using a SOR scheme for given boundary conditions (adiabatic at $r = 0$, $r = r_p$, $\theta = 0$, and $\theta = 30$ deg, fixed temperatures T_1 and T_2 at $z = 0$ and $z = r_b$). Good agreement with available experimental data was obtained up to a k_s/k_g ratio of ~150. Beyond this, the temperature drop across the solid-gas interface becomes much larger than that in the solid, creating computational difficulty. Solutions could only be obtained then for an extremely fine, tailored grid, which would be expensive computationally and impractical for repeated calculations. At the same time, the nodal temperatures inside the three-dimensional unit cell for the lower values of k_s/k_g were virtually independent of the third dimension (θ), and k_{eff} results from the three-dimensional model were essentially the same as those from the two-dimensional model (within 1%). Thus, since the solution appears to be sufficiently accurate with a two-dimensional model with much lower computational effort, the two-dimensional model was adopted for the calculations.

IV.A.2. Analysis of Experimental Results

The model was benchmarked[10,11] against experimental results available in the literature and then used to analyze the data from the experiment in Sec. III. Figures 14 and 15 show the comparison of the model predictions with experimental data[4] for k_{eff} as a function of pressure for particle diameters d_p of 0.56 and 0.12 mm, respectively. The surface properties were chosen so that the modeling results fit the data while being consistent with available surface examination. Once

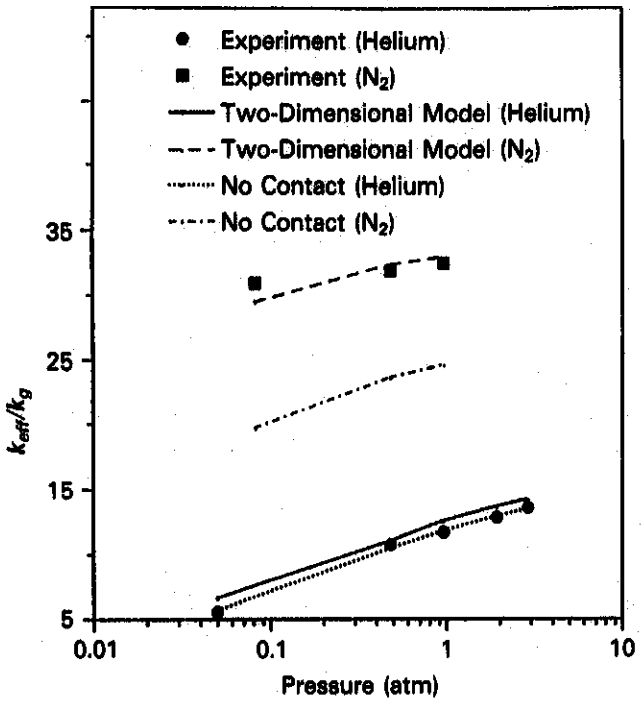

Fig. 14. Effective thermal conductivity as a function of pressure for a 0.56-mm aluminum particle packed bed of porosity 0.397 in helium ($k_s/k_g = 1300$) and N_2 ($k_s/k_g = 8000$) from Ref. 4. Modeling results are shown for $R_1/R_2 = 0.18$ and $\delta_r = 5$ μm for cases with point contact ($r_c/r_p = 0$) and a finite contact area [$(r_c/r_p)^2 = 7 \times 10^{-4}$].

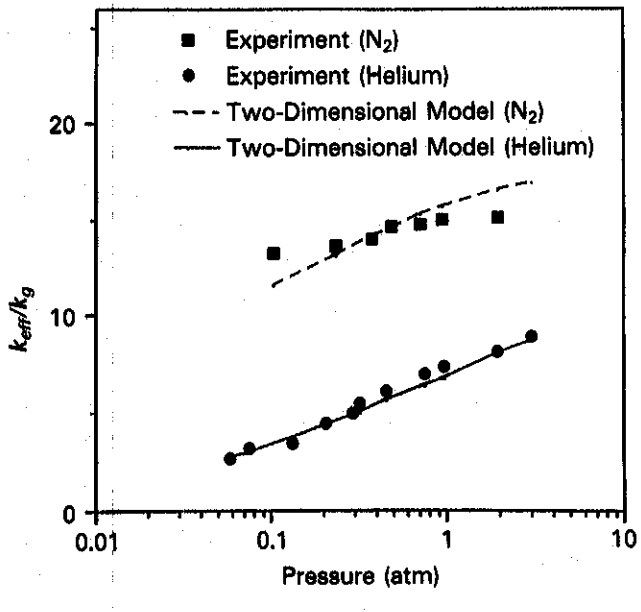

Fig. 15. Effective thermal conductivity as a function of pressure for a 0.12-mm aluminum particle packed bed of porosity 0.426 in helium ($k_s/k_g = 1300$) and N_2 ($k_s/k_g = 8000$) from Ref. 4. Modeling results are shown for $R_1/R_2 = 0.11$ and $\delta_r = 1$ μm for cases with point contact ($r_c = 0$) and a finite contact area [$(r_c/r_p)^2 = 1 \times 10^{-4}$].

a set of values for r_c, R_1/R_2, and δ_r was chosen for a particular bed, it had to be used for both the helium and N_2 cases. The modeling results agree well with the experimental data, particularly for the aluminum-helium case, which is of more interest here since its k_s/k_g ratio (~1300) is of the same order as that of beryllium-helium. The variation of k_{eff} with pressure is quite appreciable for the aluminum-helium case but, as expected, is very small for the aluminum-N_2 case with the much higher k_s/k_g ratio (~8000).

To ascertain the influence of the contact area, calculations were done for the cases with 0.56-mm particle diameter assuming zero contact area. As can be seen in Fig. 14, whereas there is a substantial reduction in the k_{eff} of the aluminum-N_2 case, k_{eff} is only slightly lower for the aluminum-helium case. This confirms that the role played by the contact area is effectively determined by the k_s/k_g ratio.

Figures 16 and 17 show the comparison of the model predictions with experimental data for binary mixtures. The chosen R_1/R_2 and δ_r values are consistent with those obtained from the modeling of k_{eff} for the single-size packed beds. The modeling results can be seen to reproduce the experimental data reasonably well. There is a substantial change in k_{eff} as the pressure increases. For example, k_{eff} at 2 atm is ~1.6 times higher than k_{eff} at 0.2 atm for the 4.3-mm + 0.12-mm case. Changing the interfacial area from $r_c/r_p = 0.01$ to 0 only slightly decreases k_{eff} but does not affect the pressure variation effect in this pressure range, as expected from the single-size k_{eff} analysis.

IV.A.3. Parametric Analysis

To better determine the effect of surface characteristics on the variation of k_{eff} with pressure, a parametric study was done with the code for the case of 0.12-mm-diam aluminum particles with $R_1/R_2 = 0.11$ (from Fig. 15) with helium. The k_s/k_g ratio is within a factor of ~2.5 higher than that for beryllium-helium, and the results are thus applicable to the beryllium-helium case of interest.

Figure 18 illustrates the results of the study. It shows the ratio of k_{eff} at 2 atm to k_{eff} at 0.2 atm as a function of the interfacial radius for different roughness heights δ_r. This ratio represents the amount of variation that k_{eff} might experience as the gas pressure is varied over a range applicable to ITER and is taken as measure of the active controllability of k_{eff}. Increasing the interfacial area should result in an increase in the heat flow through the contact region, and thus, the ratio k_{eff} (2 atm)/k_{eff} (0.2 atm) should approach unity as $(r_c/r_p)^2$ is increased, which is precisely the trend in Fig. 18. However, there is a threshold below which the contact area barely influences the pressure variation effect on k_{eff}. For this case, changing the pressure from 0.2 to 2 atm increases k_{eff} by close to a factor of 2 for contact areas corresponding to a ratio r_c/r_p up to 2.5%. The pressure effect then decreases as r_c/r_p increases until a r_c/r_p value of ~10%, beyond which there is practically no pressure effect. Based on the Hertz formula for contacting spheres under an applied load, r_c/r_p due to elastic deformation is ~0.4% for an

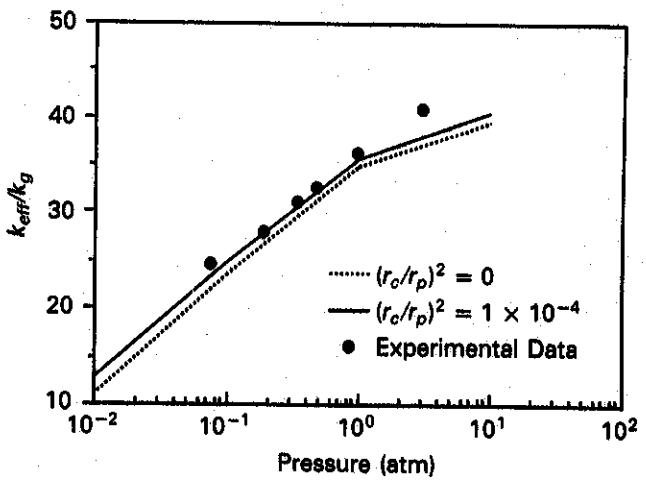

Fig. 16. Effective thermal conductivity as a function of pressure for a binary (4.3-mm + 0.56-mm) aluminum particle packed bed of porosity 0.166 in helium ($k_s/k_g = 1300$) from Ref. 4. Modeling results are shown for $R_1/R_2 = 0.15$ for the large particle and 0.18 for the small particle, $\epsilon = 0.37$ for the large particle packing, and $\delta_r/d_p = 1\%$ for cases with point contact ($r_c = 0$) and a finite contact area $[(r_c/r_p)^2 = 1 \times 10^{-4}]$.

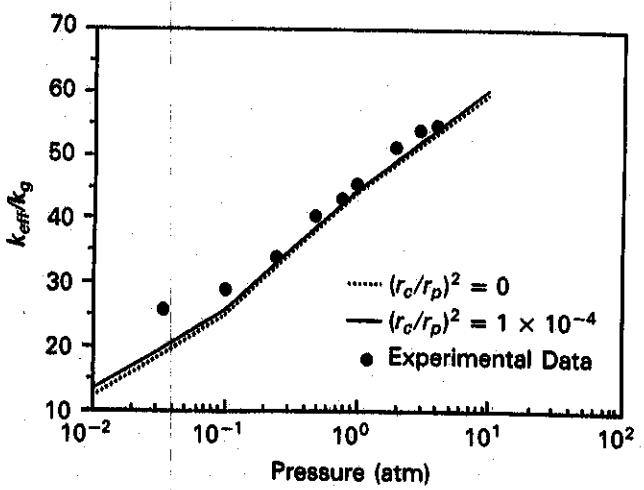

Fig. 17. Effective thermal conductivity as a function of pressure for a binary (4.3-mm + 0.12-mm) aluminum particle packed bed of porosity 0.167 in helium ($k_s/k_g = 1300$) from Ref. 4. Modeling results are shown for $R_1/R_2 = 0.15$ for the large particle and 0.11 for the small particle, $\epsilon = 0.37$ for the large particle packing, and $\delta_r/d_p = 1\%$ for cases with point contact ($r_c = 0$) and a finite contact area $[(r_c/r_p)^2 = 1 \times 10^{-4}]$.

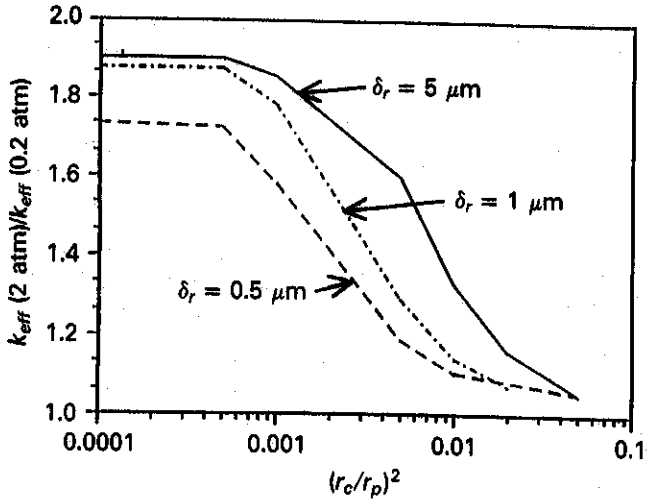

Fig. 18. Gas pressure controllability of k_{eff} of a 0.12-mm aluminum-helium packed bed ($k_s/k_g = 1300$) as a function of contact area for different surface roughnesses, for $\epsilon = 0.426$ and $R_1/R_2 = 0.11$.

assumed beryllium yield stress of 300 MPa at the contact. A larger pressure would result in plastic deformation and relief of contact pressure caused by thermal expansion and/or swelling. The overall effect on the k_{eff} controllability is unclear and would require experimental determination at prototypical conditions.

The other point to be observed from Fig. 18 is the influence of changes in δ_r. Decreasing δ_r reduces the value of the resistance at the contact region by reducing the thickness of the trapped gas particles between contacting roughnesses, thereby allowing more heat to flow through the region. This mechanism reduces the upper limiting value of k_{eff} (2 atm)/k_{eff} (0.2 atm) for a given contact radius. Increasing the contact area then reduces this k_{eff} ratio faster. In a sense, for the set of parameters considered, the higher the roughness is and the less dense its distribution over the interfacial area is, the better is the pressure controllability of k_{eff}.

The model was also used to determine how the degree of controllability of k_{eff} through gas pressure adjustment varies with the solid-to-gas thermal conductivity ratio. The ratio of k_{eff} (2 atm) to k_{eff} (0.2 atm) was used again as a measure of the controllability. As an example, the results for a single-size packed bed with 0.12-mm-diam particles are shown in Fig. 19. The controllability increases with increasing k_s/k_g up to a k_s/k_g ratio of ~500 and then decreases at higher k_s/k_g values. At these high values, most of the heat flows through solid contact points, and thus, k_{eff} is not affected by changes in gas conductivity through pressure adjustment. The exact k_s/k_g ratio at which maximum controllability is obtained depends on the bed characteristics, such as the particle size and porosity, and, for binary beds, the particle size ratio. However, it is interesting to note that for this example case, the highest controllability corresponds to a k_s/k_g ratio very close to that of beryllium and helium. This is an important result since it indicates that use of a beryllium-helium packed bed would offer excellent potential for k_{eff} control through gas pressure adjustment.

IV.B. Packed-Bed Wall Conductance

The wall conductance for a packed bed can have a noticeable effect on the temperature profile, and its relative effect becomes increasingly important as the bed thickness is reduced.

Several groups of investigators have measured and derived models for the apparent wall coefficient of heat transfer in packed beds through which gases were flowing (e.g., Refs. 16 and 17). For flowing gas, the definition of the wall heat transfer coefficient for packed beds is analogous to that of a flowing fluid in a channel and can be correlated to the Reynolds and Prandtl numbers. For stagnant fluid, however, these correlations do not usually apply.

Yagi and Kunii[18] proposed an expression for the wall conductance h_w for single-size packed beds with stagnant fluid based on the effective thermal conductivity of the bed and an effective wall thermal conductivity k_w, which is determined from one-dimensional heat transfer considerations based on an effective porosity at the wall. Another model described in Ref. 19 gives lower and upper bound estimates for the wall conductance based on parallel gas and bulk conductions over two different porosity distributions in the near-wall region. Reference 19 shows a comparison of these models with experimental data. The experimental results show wide ranges of wall conductances for similar conditions and, in the case of annular geometry, between the inner and outer walls, suggesting that h_w is determined by complex thermal behavior at the wall influenced by different parameters, which are not always

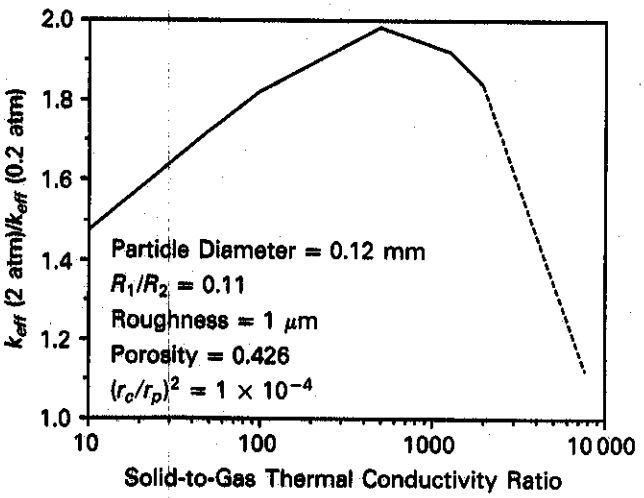

Fig. 19. Gas pressure controllability of k_{eff} of a single-size packed bed in helium as a function of k_s/k_g ratio.

well characterized. For example, the contact pressure, the porosity distribution, and the packing geometry at the wall could have substantial effects on h_w. In general, results from the models tend to fall within a factor of 2 or 3 of the experimental results, which is not unreasonable given the inherent difficulty in predicting h_w. Most experimental data fall within the lower and upper limits of the model of Ref. 19 while Yagi and Kunii's predictions tend to fall toward the lower end of the range.

Yagi and Kunii's model would not be directly applicable to binary beds, while the model of Ref. 19 would require limiting porosity distributions to be specified for binary beds. A simple lower bound expression for h_w would be useful for designers, particularly if it is applicable to binary beds. The expression could then be used to predict the maximum relative effect of the wall heat transfer coefficient on the overall bed temperature profile as a function of the bed thickness and particle size for blanket application, in particular for beryllium-helium packed beds, with high k_s/k_g ratios.

IV.B.1. Lower Bound Expression

Figure 20 shows the temperature distribution at the inner wall of a packed-bed annulus through which heat is flowing to the bed. The wall conductance is based on the difference between the actual and extrapolated wall temperatures ($\Delta T_w = T_w - T_e$), as shown in Eq. (2). From Fig. 20, the heat flux q'' at the wall can be expressed as

$$q'' = \frac{k_{eff}(T_e - T_{b1})}{x_w} = \frac{k_w(T_w - T_{b1})}{x_w} = h_w(T_w - T_e) \ , \tag{7}$$

where k_w is an effective thermal conductivity near the wall, and from Fig. 20, T_{b1} is the bulk temperature nearest the wall, which follows the bulk temperature distribution of the bed, and x_w is the wall region thickness. From Eq. (7), an expression for h_w can be derived:

$$h_w = \frac{k_w/x_w}{1 - k_w/k_{eff}} \ . \tag{8}$$

A lower limit for k_w can be set by assuming that near the wall, heat transfer occurs in series through two layers of solid and gas, respectively, set by the bed porosity ϵ:

$$k_w = \left(\frac{1-\epsilon}{k_s} + \frac{\epsilon}{k_g}\right)^{-1} \ . \tag{9}$$

In Eq. (8), x_w is set to the radius of the particle r_p to estimate h_w. Substituting Eq. (9) in Eq. (8) then yields

$$\frac{h_w r_p}{k_g} = \left(\frac{1-\epsilon}{k_s/k_g} + \epsilon - \frac{1}{k_{eff}/k_g}\right)^{-1} \ . \tag{10}$$

This expression tends to be more conservative for high k_s/k_g ratios and, thus, is better applicable to cases with $k_s/k_g > 100$, such as for beryllium-helium.[19] The expression was compared to the wall conductance values obtained from the experiments of Sec. III to verify its adequacy, and the results are shown in Table III. Note that Eq. (7) can also be applied to an annular geometry if the wall region thickness x_w is assumed to be much smaller than the thickness of the annular bed. The lower bound estimate of h_w from Eq. (10) can be seen to be appropriate for all experimental cases except for the binary bed (4.2 mm + 0.1 mm). However, even for this case, the estimate falls within the estimated experimental error of ~20%.

IV.B.2. Parametric Analysis

For simplicity, a rectangular packed-bed region, of thickness δ, is considered as part of a blanket. As a design limit, it is assumed that the thermal resistance provided by the packed-bed region should be at least f times the resistance provided by the wall conductance at the two bed interfaces, so that the thermal behavior of the overall region is dictated by the packed bed and, thus, would be less prone to uncertainties in the wall conductance values. Then, use of Eq. (10) for h_w yields

$$\frac{\delta}{k_{eff}} \geq 2fr_p\left(\frac{1-\epsilon}{k_s} + \frac{\epsilon}{k_g} - \frac{1}{k_{eff}}\right) \ . \tag{11}$$

This limit can be represented graphically by minimum values of δ/fr_p as a function of the bed porosity and the k_{eff}/k_g ratio for a given k_s/k_g ratio. For example, for a beryllium-helium packed bed at 200°C, $k_s/k_g \sim 500$, and Fig. 21 shows the minimum value of δ/fr_p required for various porosities for given values of k_{eff}/k_g. For such a binary bed with a porosity of 0.18 and with particle sizes of 1.3 mm + 0.2 mm, k_{eff}/k_g is ~ 28 based on the model in Sec. IV.A. From

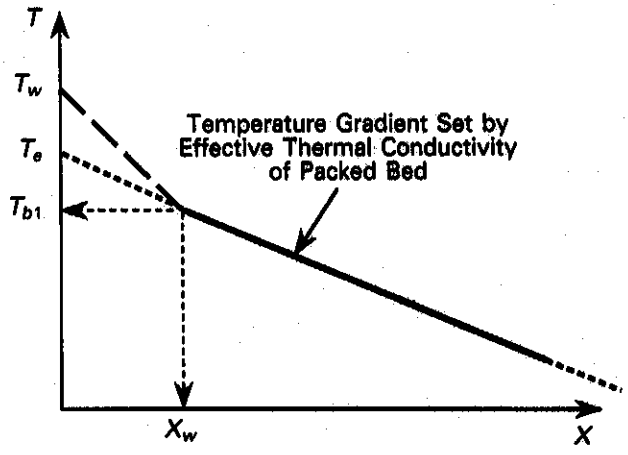

Fig. 20. Typical temperature distribution at the wall of a packed-bed region through which heat is flowing to the bed.

TABLE III

Comparison of Lower Bound Prediction of Wall Conductance* with Experimental Data from Sec. III and Ref. 7

Particle Size (mm)	Porosity	k_s/k_g	k_{eff}/k_g	$h_w r_p/k_g$	
				Experimental	Lower Limit from Eq. (10)
4.2	0.374	1300	13.1	4.8	3.4
		7800	31.0	18.9	2.9
0.5	0.376	1300	12.8	>2.34	3.4
		7800	56.2	>14.0	2.8
0.1	0.412	1300	8.75	>0.5	3.4
		7800	17.2	>2.8	2.8
4.2 + 0.5	0.14	1300	58.1	11.6	8.2
		7800	273.4	68.4	7.4
4.2 ± 0.1	0.13	1300	68.1	7.2	8.7
2 (Ref. 7)	0.39	1380	42.2	10.0	2.7
				5.1 (outer)	
			34.8	11.5	2.8
				4.1 (outer)	

[a]All measured h_w values are for the inner annular wall unless otherwise indicated.

Fig. 21, this corresponds to $\delta/fr_p \sim 8$. Thus, if it is desired to have the thermal resistance of the packed bed and, hence, the corresponding temperature drop, be five times that of the interfaces, the thickness of the bed needs to be 40 times the particle radius; in that case, ~2.6 cm. Relaxing f would decrease the required bed thickness. For a single-size bed of porosity 0.37 and 1-mm particle diameter, the model in Sec. IV.A estimates k_{eff}/k_g as being ~11, and δ/fr_p from Fig. 21 is ~6. For $f = 5$, the required minimum bed thickness is 30 times the particle radius, or ~1.5 cm.

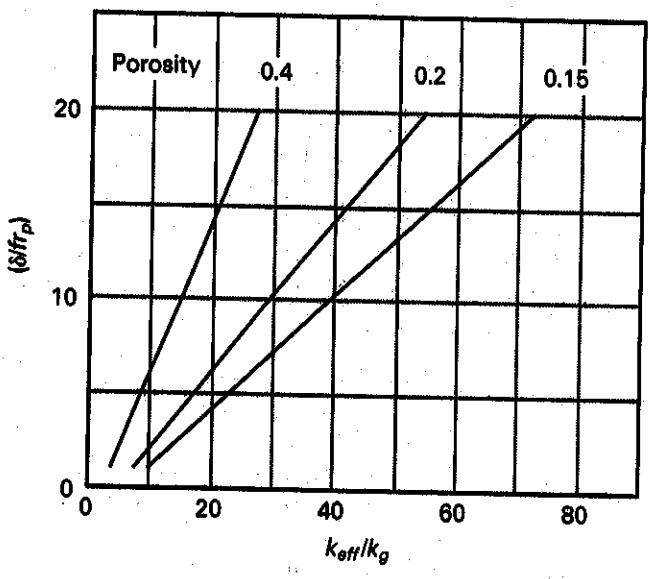

Fig. 21. Minimum values of the ratio of bed thickness to particle radius as a function of k_{eff}/k_g and porosity for $k_s/k_g = 500$. A factor f is included, representing the ratio of bed-to-interface thermal resistance.

IV.C. Beryllium–Stainless Steel Interface Contact Resistance

To fully assess the thermal performance of blankets utilizing sintered blocks of beryllium or ceramic breeder, including their ability to accommodate power variation, the thermal resistances of the beryllium-cladding and ceramic breeder–cladding contacts need to be characterized. Reference 20 describes in detail a study of the factors affecting the gas and solid conductances in the contact zone based on the semiempirical models of Lemczyk and Yovanovich[21] and Shlykov et al.[22] These models were chosen as representative of the better models available from the literature. Here, the results are briefly reported.

Both models express the total interface conductance as the sum of the effective gas and solid conductances. Key parameters affecting the gas, solid, and total conductances at the solid-to-solid interface include the gap thickness, the surface roughness, the material hardness, and tensile stress. The effect on the interface conductance of each of these parameters is discussed below.

IV.C.1. Parametric Analysis

The gap thickness at the beryllium-steel interface could vary during operation because of swelling and

thermal expansion and, thus, could have a significant effect on the thermal performance of ceramic breeder blankets utilizing beryllium sintered blocks. The gap thickness in combination with the roughness represents the characteristic heat conduction length. The ratio of the gas mean free path to the characteristic heat conduction length gives the Knudsen number Kn, whose value determines the heat conduction regime through the gas. For a very small Kn ($\sim 10^{-3}$ and lower), the gas can be treated as a continuum, and ordinary conduction occurs. As Kn is increased, noncontinuum effects play an increasing role until conduction is fully in the molecular regime. For helium at 1 atm and 400°C, a gap thickness of ~ 250 μm or more is required for Kn to be $\sim 10^{-3}$ or lower and for ordinary conduction to prevail.

The corresponding gas conductance based on the model of Lemczyk and Yovanovich is shown in Fig. 22 as a function of the gap thickness t_{gap} and the beryllium roughness for a steel roughness of 1 μm. For $t_{gap} = 0$, the gas conductance is effectively a function of the roughness only and is much higher for the lower roughness value. It then decreases rapidly as t_{gap} is increased and is in effect inversely proportional to t_{gap} at higher gap thicknesses where the roughness is relatively too small to have any significant effect.

Mechanical properties of the contacting materials, particularly the hardness and the tensile stress, can affect the interface conductance. Lemczyk and Yovanovich include the ratio of contact pressure to microhardness (P_c/H_{eff}) in their expression for determining both the gas and solid conductances for solid-to-solid contact. Shlykov et al. do not include mechanical properties in the determination of the gas conductance but express the solid conductance as a function of the ratio of contact pressure to the ultimate tensile strength ($P_c/3S_{ft}$).

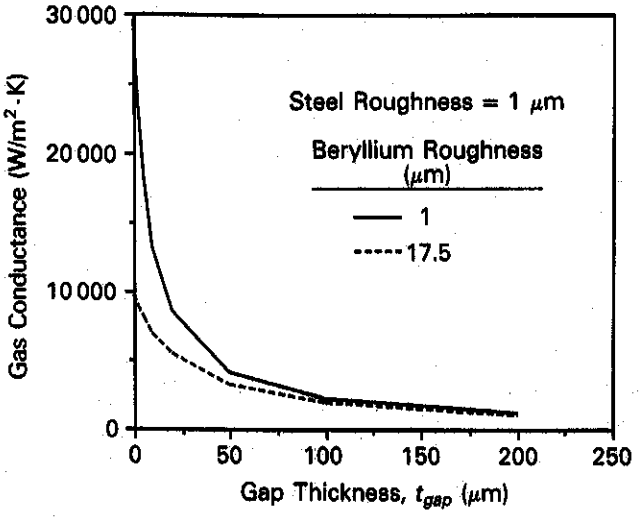

Fig. 22. Gas conductance as a function of gap thickness for different beryllium roughnesses.

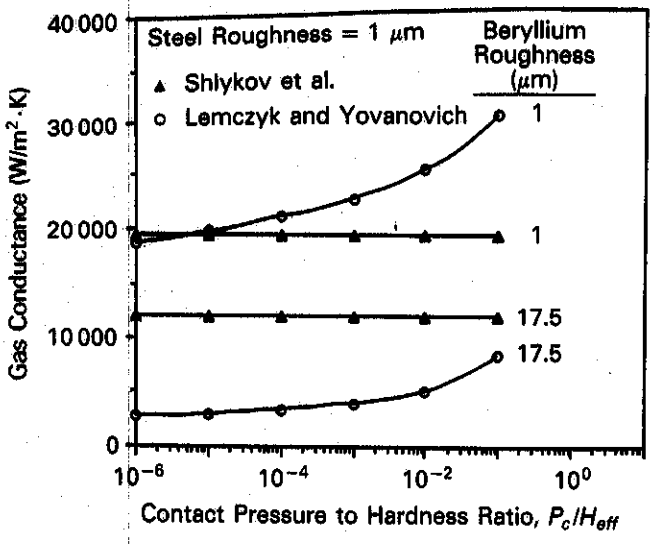

Fig. 23. Gas conductance as a function of beryllium-steel contact pressure to hardness ratio for different beryllium roughnesses.

Based on Refs. 22 and 23, $3S_{ft}$ can be considered as a rough representation of H_{eff}, which is assumed here. This assumption is very helpful when analyzing cases with beryllium since data on its ultimate tensile strength are more readily available than data on its hardness.

Figure 23 shows the effect of the P_c/H_{eff} ratio on the gas conductance based on the Lemczyk and Yovanovich model for zero gap thickness, a steel roughness of 1 μm, and beryllium roughnesses of 1 and 17.5 μm. The gas conductance can be seen to increase with P_c/H_{eff}. As a means of comparison, corresponding estimates of the gas conductance based on the model of Shlykov et al. are also shown. For P_c/H_{eff} ratios of up to at least 0.1, the Lemczyk and Yovanovich predictions are decreasingly lower than those of Shlykov et al. for a beryllium roughness of 17.5 μm and increasingly higher for a beryllium roughness of 1 μm. Both models indicate that the gas conductance is much higher for the smoother surface.

Figure 24 shows the effect of the P_c/H_{eff} ratio on the solid conductance based on both models. Both models show the solid conductance increasing with decreasing roughness, and both indicate a sharp increase in solid conductance when the P_c/H_{eff} ratio reaches a value of $\sim 10^{-2}$ to 10^{-3}, especially for the lower beryllium roughness. Figure 25 shows the effect of P_c/H_{eff} on the total contact conductance as a summation of the gas and solid conductances based on both models for beryllium roughnesses of 1 and 17.5 μm. Under both models, the total conductance behaves similarly to the solid conductance for higher values of P_c/H_{eff}, with a substantial increase observed when P_c/H_{eff} reaches $\sim 10^{-2}$, in particular for the low beryllium roughness case.

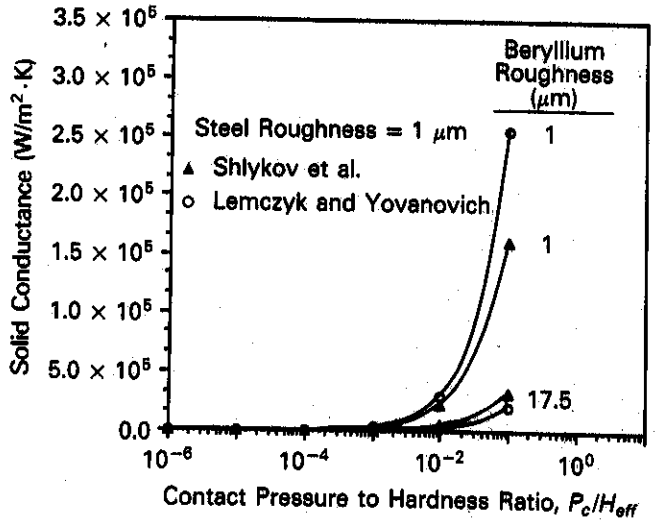

Fig. 24. Solid conductance as a function of beryllium-steel contact pressure to hardness ratio for different beryllium roughnesses.

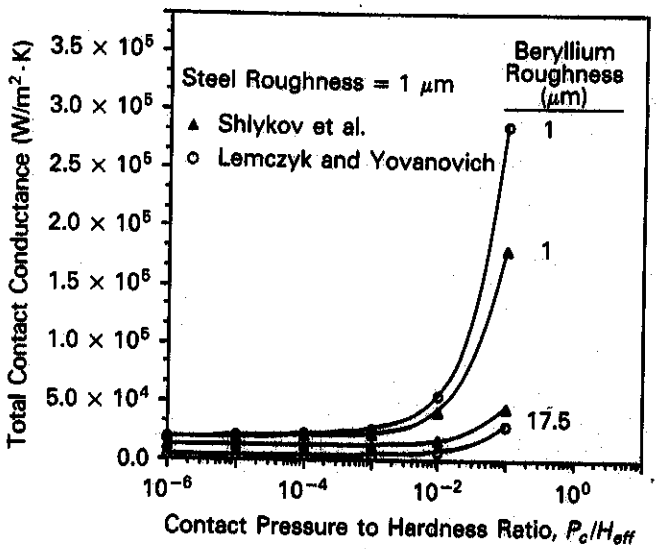

Fig. 25. Total contact conductance as a function of beryllium-steel contact pressure to hardness ratio for different beryllium roughnesses.

This indicates that the contribution of the solid conductance becomes dominant when the P_c/H_{eff} ratio reaches $\sim 10^{-2}$ depending on the roughness. It is interesting to note that for a beryllium roughness of 17.5 μm, the largest difference between the two model predictions occurs at low values of P_c/H_{eff}, the model of Shlykov et al. predicting a total conductance value about four times larger than that of Lemczyk and Yovanovich for a P_c/H_{eff} of 10^{-6}. For a beryllium roughness of 1 μm, the largest difference occurs at higher values of P_c/H_{eff}, Lemczyk and Yovanovich's prediction being $\sim 50\%$ higher than that of Shlykov et al. for a P_c/H_{eff} of 0.1.

IV.C.2. Effect of Operating Conditions

Operating conditions can significantly affect the thermal conductance of the beryllium-steel interface. In this section, effects on this interface conductance from temperature, mechanical bending, and mechanical constraint of beryllium blocks are examined.

Figure 26 shows the effect of temperature on the beryllium-steel effective solid thermal conductivity, the beryllium ultimate tensile strength, and the resulting solid contact conductance, normalized to their respective values at 300 K for beryllium and steel roughnesses of 1 μm. The solid thermal conductivity increases with temperature while the ultimate tensile strength decreases, but their combined effect causes the solid conductance to markedly increase with temperature. For example, raising the temperature from 500 to 700 K causes an $\sim 14\%$ increase in the solid thermal conductivity and a 9% decrease in S_{ft}, which result in an $\sim 28\%$ increase in the solid conductance. Note that the relative increase of the solid conductance is about the same for both models. The results are in reasonable agreement with experimental data on the temperature effect on stainless steel–stainless steel contact conductance (with roughnesses of 0.7 and 1.2 μm) (Ref. 24).

These results are quite beneficial when applied to the blanket design since an increase in temperature results in an increase in conductance due to the combined temperature effects on conductivity and ultimate

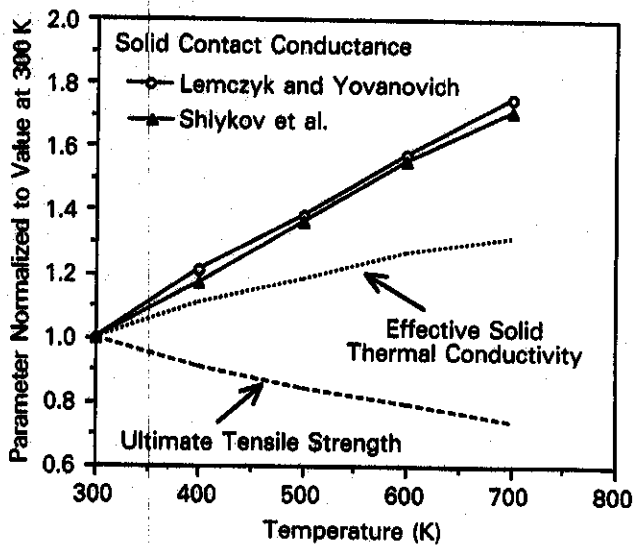

Fig. 26. Influence of temperature on the effective solid thermal conductivity, beryllium ultimate thermal strength, and the resulting solid contact conductance of the beryllium–stainless steel interface (normalized to their values at 300 K).

strength. This could reduce the temperature drop at the interface, thereby allowing higher temperature operation and passive power accommodation based on maintaining the ceramic breeder temperature within its allowable window.

In the design, each beryllium sintered block will experience a thermal gradient. If the blocks are not constrained, they will curve to relieve the stress due to differential thermal expansion, resulting in a slight deflection at the beryllium–stainless steel interface. The effect of the maximum bending deflection Δ_{max} on the beryllium–stainless steel interface solid conductance was estimated from Malkov et al.'s comparison of *in vacuo* experimental data with Shlykov et al.'s model predictions.[23] This relative change is a function of the ratio of Δ_{max} to the sum of the surface roughnesses.

Figures 27 shows the effect of Δ_{max} on the total conductance for a beryllium-steel interface for different P_c/H_{eff} ratios and beryllium. When Δ_{max} is increased from 0 to 50 μm, the total conductance decreases substantially, to an extent depending on the roughness and P_c/H_{eff} ratio. This is an important result since it suggests that a 50-μm bending deflection can increase the contact temperature drop by up to a factor of 5 assuming full contact initially and must be considered when characterizing blanket performance under different temperature levels.

Finally, the effect of thermal expansion or swelling on fully constrained beryllium blocks is considered as a limiting case by assuming that the constrained expansion results in higher stresses and, hence, on higher contact pressure at the beryllium-steel interface.

The following expression was used:

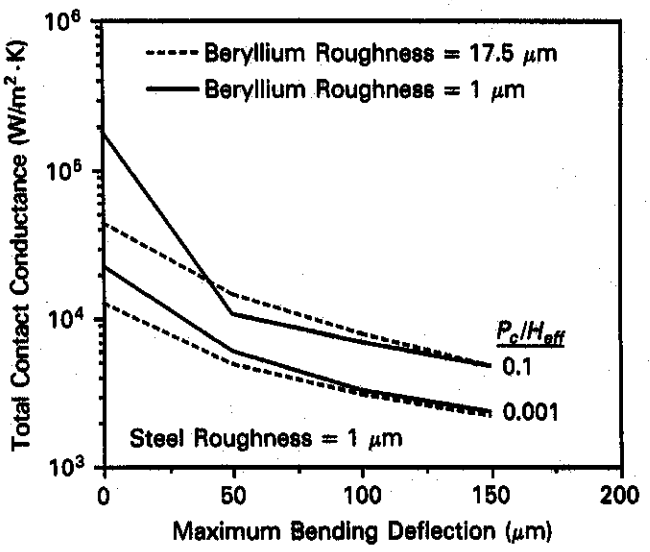

Fig. 27. Total contact conductance ratio as a function of beryllium maximum bending deflection and beryllium-steel contact pressure-to-hardness ratio for different beryllium roughnesses.

$$P_c = \frac{E}{3(1-2\nu)} \frac{\Delta V}{V} , \qquad (12)$$

where

E = Young's modulus

ν = Poisson's ratio

$\Delta V/V$ = volumetric strain for beryllium.

The calculations show that for this limiting fully constrained case, a volumetric expansion of only ~0.6% causes $P_c/3S_{ft}$ to be 1. In a design, space would have to be provided to accommodate volumetric expansion, and in addition, the cladding would probably deflect under excessive pressure at the contact point. Thus, the effective volumetric expansion causing the pressure would be significantly lower than the actual volumetric expansion. The benefit of increasing contact pressure due to any constrained expansion can be seen from Fig. 25, where the total conductance increases significantly with increasing P_c/H_{eff}, particularly for lower roughnesses.

V. THERMAL CONTROL ANALYSIS

In this section, the thermal control performance of the four different configurations described in Sec. II are analyzed and assessed in light of the results from Secs. III and IV. The analysis includes determination of key uncertainties and of the possibility of active thermal control. As part of the assessment, the allowable wall load range was estimated for each case as a function of the thermal control region thickness δ from Fig. 1, based on example calculations using the assumptions listed below:

1. Li_2O as ceramic breeder and water as coolant
2. a heat generation of 20 MW/m^3 in the ceramic breeder, which is typical of the ceramic breeder region behind the first wall for a neutron wall loading P_N of 1.2 MW/m^2
3. a ceramic breeder layer thickness of 1 cm, which results in a heat flux of 0.1 MW/m^2 to the thermal resistance region and a temperature drop of 100 K across the ceramic breeder
4. maximum and minimum allowable temperatures of 673 and 1273 K for the ceramic breeder, which is compatible with the operating temperature window of Li_2O based on sintering and LiOT mass transport considerations for the higher temperature limit and LiOT precipitation and solubility considerations for the lower temperature limit
5. a constant coolant temperature of 343 K
6. a convective heat transfer coefficient of 3300 W/m^2·K.

these two ranges depending on the emissivity of the surfaces.

The blanket operating flexibility could be increased if a means of active control of the thermal resistance region were provided. For a helium gap, two possible means of controlling its conductance are: (a) a change in gas pressure, provided conduction occurs at least in part in the Knudsen regime, and (b) a change in the gas flow rate if the helium could be flowed, provided the corresponding pressure drop is reasonable.

V.A.1. Pressure Control

The possibility of helium thermal conductivity control through pressure adjustment was assessed. Conduction must take place at least in part in the molecular regime for pressure to affect the helium thermal conductivity, and thus, the characteristic conduction distance with respect to the gas mean free path becomes a key factor. The thermal conductivity of helium was calculated for different pressures and gap distances assuming an average temperature of 573 K according to Eqs. (4) and (5). It is believed that for reactor application, the lowest practical operating pressure for helium is of the order of 0.1 atm, and the ratio of thermal conductivity at 1 atm to that at 0.1 atm is used as a measure of active thermal control. The upper pressure of 1 atm is chosen since even for the smallest gap thickness considered (0.1 mm), the thermal conductivity tends to saturate at about this pressure. The results are illustrated in Fig. 29. The pressure control of the thermal conductivity is quite high for a gap thickness of 0.1 mm (~47%) but decreases rapidly as the thickness is increased. For a practical gap thickness of ~1.5 mm, the control is negligible (<2%). In addition, even for cases with smaller gap thicknesses, where the thermal conductivity can be significantly varied with pressure adjustment, the resulting control of the ceramic breeder temperature is also small since the adjustable temperature drop through the thinner gap is lower. For example, based on the assumptions mentioned earlier, the temperature drop was calculated as a function of the gap thickness, and it is also shown in Fig. 29. It can be seen that while the degree of thermal conductivity control increases with decreasing gap thickness, the gap temperature drop decreases, and the two effects at least partially cancel each other, so that for this case, the allowable power variation provided by active control is always <2% even for the 0.1-mm gap. This indicates that pressure adjustment of helium resistance gaps can be effectively ruled out as an active control mechanism for ITER blanket application.

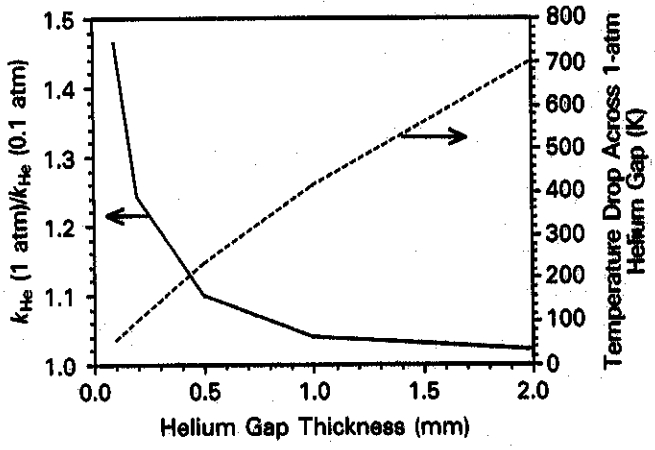

Fig. 29. Ratio of helium thermal conductivity at 1 atm to helium thermal conductivity at 0.1 atm as a function of the helium gap thickness. The temperature drop across the helium gap is also shown assuming a heat flux of 0.1 MW/m^2 from the ceramic breeder region to the helium gap. (For helium, the following parameter values were used: $\alpha = 0.4$, $\gamma = 1.67$, Pr = 0.67, $\lambda_{std} = 1.74 \times 10^{-7}$ m.)

V.A.2. Flow Rate Control

To assess the possibility of thermal control through flow rate adjustment for flowing helium, the variation of the Nusselt number Nu with the Reynolds number Re was considered. For laminar flow, heat transfer occurs mostly through conduction. For the blanket case, a fully developed profile is a reasonable assumption since the entry length even for a high laminar Re of 2000 is only of the order of 10 cm for a 1-mm gap. In this case, the Nu for parallel plates at two different temperatures is 4 for each wall.[26] The effective conductance of the region can be estimated as the combination of two heat transfer coefficients based on the effective resistance of two resistances in series. For that case, a Nu of 4, based on the hydraulic diameter (~$2\delta_{He}$), corresponds to the conductance of a stagnant helium region. Thus, it appears that little active control can be achieved through flow variation in the laminar regime.

In the turbulent regime, Nu increases substantially with increasing Re; however, the corresponding pressure drop also increases. For a Re of 10^4, Nu based on the Dittus-Boelter correlation[27] is 31, which results in significantly lower thermal resistance than the stagnant gap; however, the pressure drop based on the Moody chart friction factor[27] is >2 atm/m for a 2-mm gap and jumps to 17 atm/m for a 1-mm gap. In general, the helium gap pressure should be lower than the coolant pressure to minimize tritium contamination to the coolant in case of leakage. For cases such as the ITER blanket where for safety and reliability reasons, the coolant can be kept at a low pressure of a few atmospheres, the pressure drop for turbulent helium flow in a 2-mm gap is unacceptable.

This discussion indicates that significant active control through flow rate variation in a helium gap is possible only for cases with high coolant pressure. A

trade-off between the advantages of such a scheme, including the possibility of using turbulence-enhancing mechanisms, and the problems raised by having high pressure and a pressure drop in the helium gap should be made for specific cases.

V.B. Beryllium Region

V.B.1. Beryllium Sintered Block

One of the concerns with the use of beryllium sintered blocks relates to the beryllium block deflection under free differential thermal expansion and its resulting effect on the thermal resistance at the beryllium-cladding interface, as mentioned in Sec. IV.C.2. Full constraint of the beryllium block to prevent such a deflection could result in high stresses and a significant amount of additional structure. For example, for a beryllium thickness of 5 cm, a beryllium temperature drop of 260 K, and a beryllium block length of 1 m, the free deflection is of the order of 1 cm, and full constraint of the beryllium block would require a rigidly supported cladding of thickness of >1 cm and would result in stresses of ~230 MPa in the beryllium. To remedy this concern, the beryllium region would have to consist of a number of small adjacent blocks with or without a thin common base. The small block thickness should be the same as the beryllium region thickness to avoid beryllium block interfaces in the direction of heat flow, which would add uncertainty to the overall region thermal resistance during operation. The width and length of the blocks would be set according to an acceptable level of block deflection, which for a block of dimensions $a \times a \times \delta$, where δ is the thickness, would vary with a^2/δ. If the small blocks were free, they would have to be stacked so as to allow for differential lateral movement between them. Otherwise, friction might prevent each block from moving freely, the block assembly would behave as a single large block, and the resulting deflection will still be high. Tapering of the blocks would help reduce or eliminate the friction force between them, particularly if a common base is used, resulting in a "chocolate bar" configuration.[28]

Sensitivity studies of the multilayered blanket with sintered beryllium blocks were done to evaluate the effect of helium gap formation at the beryllium-cladding interface due to differential thermal expansion.[2] For this design, the gap thickness tended to increase with the beryllium region thickness so that the effect on the overall beryllium region conductance was within 20% and could be comfortably tolerated because of the wide ceramic breeder temperature window.

Another concern that also brings uncertainty to the thermal resistance performance of the beryllium sintered block region is the beryllium-cladding interface resistance, as discussed in Sec. IV.C. Under controlled conditions, this resistance can be predicted from existing models based on a number of parameters, including the thermal conductivity, hardness and roughness of each material, and the contact pressure. The smaller the contact resistance is, the smaller is its effect on the overall beryllium region thermal resistance and, in turn, on the ceramic breeder temperature. Thus, for cases where the contact pressure is high, such as when the beryllium swells inside the cladding, uncertainties in predicting the contact resistance are not so important since the contact temperature drop is low. However, cases where the contact pressure is small and, even more, where actual separation occurs are of concern, particularly when considering that the thermal conductivity of helium is lower than that of beryllium by a factor of ~400, depending on the temperature.

The range of allowable wall loading based on the allowable temperature window of the ceramic breeder was calculated for the beryllium sintered block case also using the assumptions listed at the beginning of Sec. V. In addition, the heat generation in the beryllium was set at 3 MW/m^3 for a wall loading of 1.2 MW/m^2, and the contact conductance at the beryllium-cladding interfaces was set at 2000 W/m^2·K based on Fig. 25 under the assumptions of contact under a normalized pressure, $P_c/H_{eff} < 10^{-2}$, and a roughness of ~17.5 μm or more. Equations similar to Eqs. (14), (15), and (16) but with additional terms for temperature drops at the two beryllium-cladding interfaces were used. The helium average temperature and thermal conductivity were replaced by those of the beryllium sintered block region. In contrast to the helium case, the thermal conductivity of beryllium tends to decrease exponentially with increasing temperature within the temperature range of interest (shown as part of Fig. 32), which limits the range of allowable wall loading.

The results are shown in Fig. 30. Note that any uncertainty in the parameters affecting the ceramic breeder temperature would effectively reduce the allowable wall load range shown in the figure. For a minimum wall load of 1.2 MW/m^2, the required beryllium region thickness is ~4.2 cm, with a corresponding maximum allowable wall load of 2.4 MW/m^2. A maximum wall load of 1.2 MW/m^2 is allowable for a beryllium region thickness of ~8.6 cm, and the corresponding minimum allowable wall load is 0.62 MW/m^2. A thickness of ~5.3 cm would enable accommodation of a reasonable wall load range of 1 to 2 MW/m^2. Thus, the passive accommodation of power variation in this case tends to be lower than in the pure helium gap case.

V.B.2. Beryllium Sintered Block with Metallic Felt

One of the advantages of placing a felt at the beryllium-cladding interface is the possible provision of a means of active control based on the variation of the thermal conductivity of the felt region with gas pressure. The effect of gas pressure on the thermal conductivity of the felt was estimated by applying the thermal

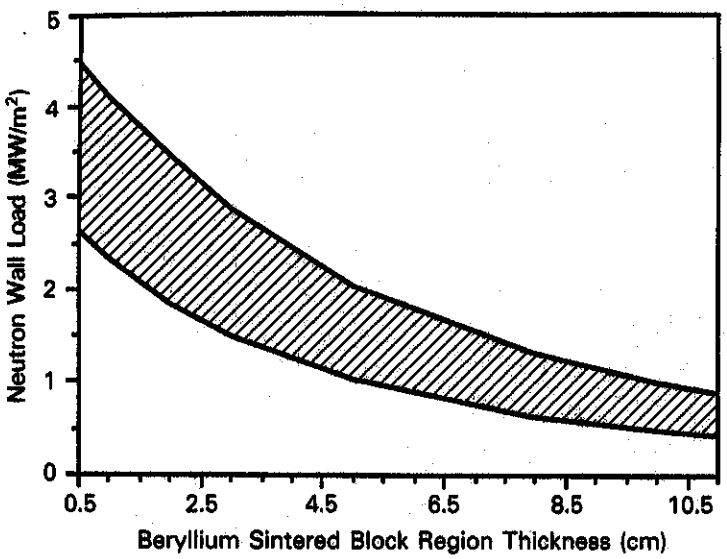

Fig. 30. Range of allowable wall loads based on the ceramic breeder temperature limits as a function of the thickness of the beryllium sintered block region between the ceramic breeder and water coolant.

conductivity model of Kunii and Smith[8] for porous material to the felt case. A simple rectangular configuration was assumed for the felt fibers, and the gas characteristic distance was estimated as a function of the porosity for an assumed fiber diameter of 8 μm and used to calculate the interstitial gas conductivity as a function of pressure in the model. For a Type 316 stainless steel felt and helium, the effective thermal conductivity of the felt at 1 atm is ~2.7 W/m·K for a felt porosity of 15% and 1.3 W/m·K for a felt porosity of 40%. The ratio of felt thermal conductivity at 1 atm to felt thermal conductivity at 0.1 atm is estimated at ~1.6 for a felt porosity of 15% and at ~1.7 for a felt porosity of 40%.

The extent of active thermal control provided by the felt is dependent on its initial temperature drop and, thus, on its thickness. The felt could be positioned at either or both beryllium-cladding interfaces. Placing the felt at the high-temperature interface would minimize the beryllium temperature, which is desirable for swelling considerations. However, placing the felt at the low-temperature interface would maximize the heat flux through the felt and, consequently, the active thermal control provided by control of the felt thermal resistance. The latter case is assumed in the example calculation for the thermal control provided by the felt. The contact conductance at the high-temperature beryllium-cladding interface is still assumed to be 2000 W/m²·K, and the other assumptions used in the previous calculations are maintained for consistency.

Figure 31 shows the active control provided by the felt as a function of the felt thickness for a case where the beryllium sintered block thickness without the felt is 5.3 cm (see Fig. 30). The controllability is calculated from the ratio of felt thermal conductivity at 1 atm to that at 0.1 atm and is used to estimate the lower limit of allowable wall loading while the maximum allowable wall load is kept at 2 MW/m².

Including a felt at the beryllium-cladding interface can provide significant active control, lowering the allowable wall loading from 1 MW/m² for the case without the felt to ~0.7 MW/m² for a case with a felt thickness of 2 mm. The corresponding beryllium sintered block thickness is 2.2 cm, a substantial reduction from the original 5.3-cm thickness without the felt.

V.B.3. Beryllium Packed Bed

Figure 32 shows the effective thermal conductivity k_{eff} of a single-size and a binary beryllium-helium packed bed at 1 atm as a function of temperature based on calculations from the model described in Sec. IV.A. Also shown are the helium and beryllium thermal conductivities. As noted earlier, the beryllium thermal conductivity decreases with temperature, while the helium thermal conductivity increases, resulting in a slight increase in effective thermal conductivity with temperature for both packed beds, which was incorporated in the example calculation described in this section.

Recent data and modeling analyses discussed in Secs. III and IV.A have confirmed the sharp effect of gas composition changes and pressure on the k_{eff} of a beryllium-helium packed bed. For example, changing from N_2 to helium would increase the k_{eff} of a beryllium-helium packed bed by up to a factor of 3. However, for blanket application, irradiation and compatibility effects would substantially limit the choice of available gases, and gas composition changes could significantly increase the complexities of the purge system.

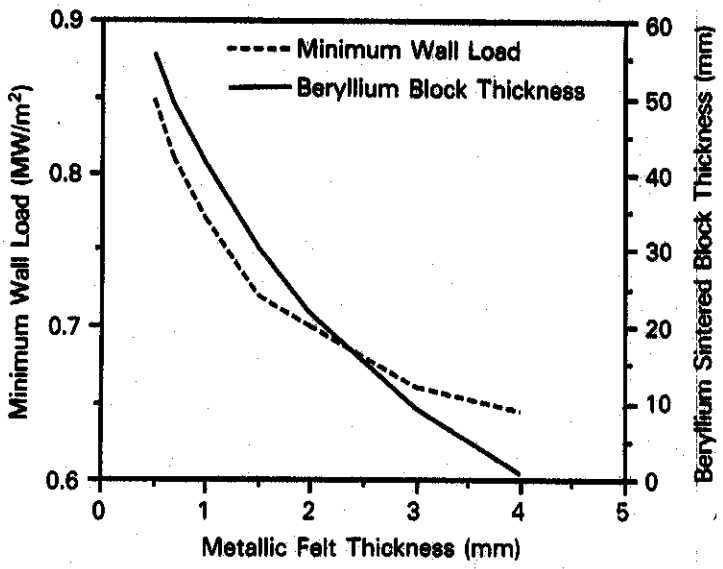

Assumptions

T_{water} = 343 K
$h_{contact}$ = 2000 W/m²·K
Allowable minimum solid breeder temperature = 673 K
For 1.2 MW/m² wall load
q''_{CB} = 0.1 MW/m²
q'''_{Be} = 3 MW/m³
ΔT_{film} = 30 K
Metallic Felt
k = 1.3 W/m·K at 1 atm
$k_{(1\ atm)}/k_{(0.1\ atm)}$ = 1.7

Fig. 31. Minimum allowable wall load as a function of Type 316 stainless steel felt thickness for the case where the sintered block thickness without the felt is 5.3 cm (see Fig. 30) and the maximum allowable wall load is kept at 2 MW/m². The corresponding beryllium sintered block thickness to provide the required thermal resistance is also shown.

For these reasons, gas pressure adjustment might be more attractive for blanket application.

Changing the helium pressure from ~0.1 to ~1 atm would increase the beryllium-helium packed-bed k_{eff} by up to a factor of 2. This was used in the example calculations presented here. These calculations are similar to the previous ones for the helium gap with additional assumptions of a binary bed and a packed-bed wall conductance set at 1000 W/m²·K, corresponding to a conservative value of $h_w r_p/k_g$ of ~2.2 (see Table III). Equations similar to Eqs. (14), (15), and (16) but with the helium average temperature and thermal conductivity replaced by those of the beryllium-helium packed bed were used. Additional terms for the temperature

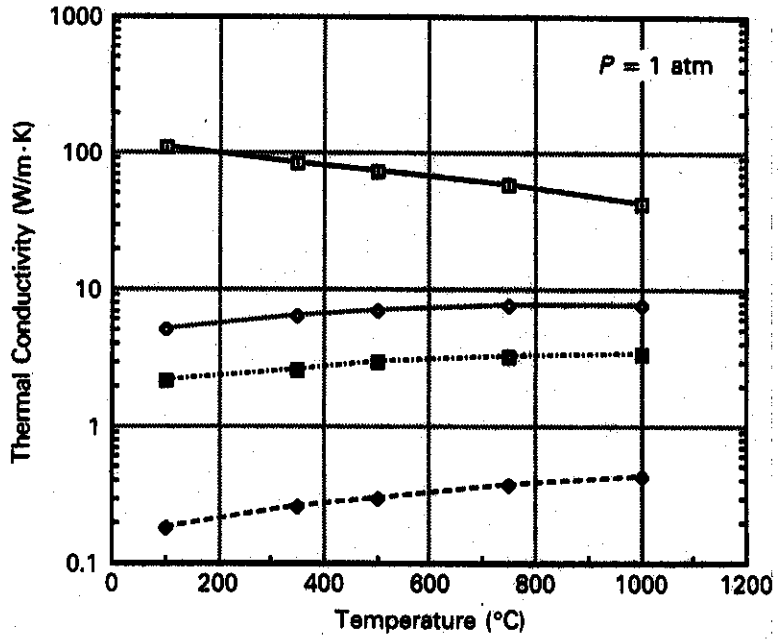

Beryllium (0.85 TD)
Binary Be/He
Single-size Be/He
Helium

For Be/He Packed Beds:
Binary
1.3 mm + 0.2 mm, Porosity = 0.18,
$r_{contact}$ = 0
Single Size
1 mm, Porosity = 0.37
$r_{contact}$ = 0
Roughness = 5 μm

Fig. 32. Thermal conductivity of beryllium, helium, and single-size and binary beryllium-helium packed beds (neglecting radiation) as a function of temperature.

drops at the two packed-bed–wall interfaces were also included. The active control was calculated by increasing the temperature drop across the beryllium bed region thickness by the k_{eff} controllability factor of 2 in the calculation of f_{min}. The results are shown in Fig. 33 in terms of the allowable neutron wall load range as a function of the beryllium packed-bed region thickness, based on both passive and active thermal control.

In this case, the bed thickness is 1 mm for a minimum allowable wall load of 1.2 MW/m^2, with a corresponding maximum value of 3 MW/m^2. A bed thickness of ~2.2 cm results in a maximum wall load of 1.2 MW/m^2, with a corresponding minimum value of ~0.3 MW/m^2. As compared with the results for the sintered block form, shown in Fig. 30, the packed-bed form seems to offer a wider allowable wall loading range, relevant to ITER. For example, for a packed-bed thickness of 1 cm, the passive wall load range is ~0.82 to 2.0 MW/m^2, while active control enables operation at a lower wall load of 0.58 MW/m^2. Note that the allowable neutron wall load range would appreciably increase if the wall conductance were higher than the assumed value of 1000 W/m^2·K. Also note that the region thickness is limited by the size of the beryllium particles. For the binary bed considered, at 400°C from Fig. 32, k_{eff}/k_g is ~24. From Fig. 21, for a porosity of 0.18, δ/fr_p is conservatively ~6. Thus, for a bed thickness of 2.2 cm and a particle diameter of 1.3 mm, the bed-to-interface thermal resistance ratio f is 5.6. This is reasonable, and the overall region thermal resistance would then be mostly governed by the bed thermal resistance. Different particle sizes or requirement for the f ratio could significantly change the desirable bed thickness and should be considered carefully for design application.

VI. CONCLUSIONS

Thermal control is an important issue for ceramic breeder blankets since the breeder needs to operate within its temperature window for the tritium release and inventory to be acceptable. A thermal control region is applicable not only to situations where the coolant can be run at low temperature, such as for the ITER base blanket, but also to ITER test module and power reactor situations, where it would allow for ceramic breeder operation over a wide range of power densities in space and time.

VI.A. Conclusions from Experimental and Modeling Studies

Experimental and modeling studies of thermal control of ceramic breeder blankets were performed. The experiments consisted of the determination of the thermal behavior of metallic packed beds to simulate beryllium beds that could be used in ceramic breeder fusion reactor blankets. Data were presented for a range of helium and N_2 gas pressures, for several single-size and binary beds of aluminum, and for a number of different porosities. In parallel, a two-dimensional model was developed for estimating k_{eff}. Its capabilities include accounting for single-size and binary beds, finite contact area, surface roughness, and pressure effect through gas conduction in the Smolukovski regime. It was calibrated from experimental data found in the literature and then used to analyze the experimental

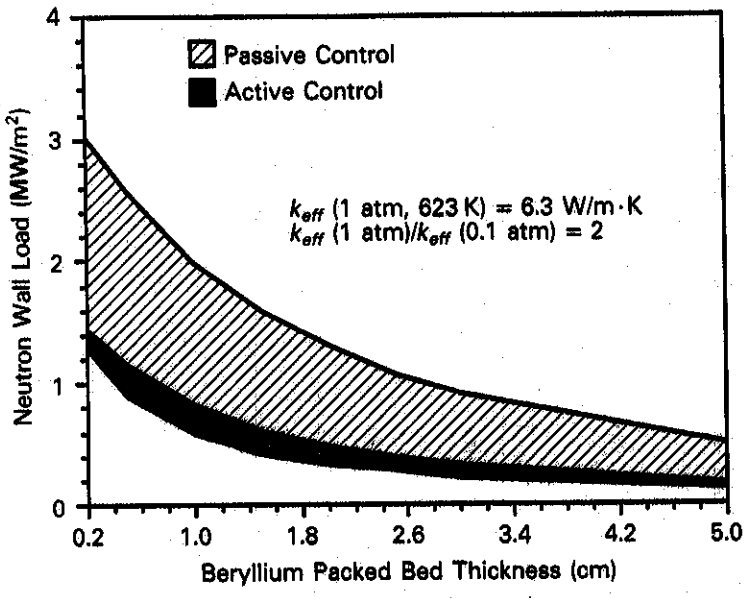

Assumptions
T_{water} = 343 K
h_w = 1000 W/m^2·K
Allowable ceramic breeder T_{min} = 673 K
Allowable ceramic breeder T_{max} = 1273 K
For 1.2 MW/m^2 wall load
ΔT_{CB} = 100 K
q''_{CB} = 0.1 MW/m^2
q'''_{Be} = 2.5 MW/m^3
ΔT_{film} = 30 K
Binary 1.3 + 0.2 mm bed
packing fraction = 0.82

Fig. 33. Range of allowable wall loads based on the ceramic breeder temperature limits as a function of the thickness of the beryllium packed-bed region between the ceramic breeder and water coolant.

results. In addition, modeling studies were carried out for beryllium packed-bed wall conductance and beryllium sintered block–stainless steel contact resistance. From the results, the following observations can be made:

1. The effective thermal conductivity of the packed beds shows substantial variation with gas pressure—as much as a factor of 3 in some cases. Results from the model indicate that the maximum pressure controllability of k_{eff} for a single-size bed (based on the ratio of k_{eff} at 2 atm to k_{eff} at 0.2 atm) is obtained with a k_s/k_g ratio of ~400 to 500. This is an important result since this k_s/k_g ratio corresponds to that of beryllium-helium, which indicates the potential of active control of a beryllium-helium bed for ceramic breeder blanket application.

2. The k_{eff} also varies substantially with gas composition change, up to a factor of 3 when changing from N_2 to helium.

3. The k_{eff} for packed beds is very sensitive to the packing fraction based on experimental results. In addition, factors such as the contact area, surface characteristics, and oxide layer can significantly affect k_{eff}. It is believed that a combination of these factors is responsible for the tendency of the experimental results to be lower than those from the literature for single-size packed beds with different materials but with about the same k_s/k_g ratio and for aluminum-helium beds at 1 atm. However, trends such as the variation of k_{eff} with pressure and gas composition are similar. It appears then that for blanket application, experimental measurements must be done with prototypical materials under prototypical packing techniques and operating conditions.

4. In most experimental cases, the wall temperature jump is relatively small compared with the temperature difference across the bed. The relative effect is smallest in single-size beds with smaller particles. The variation of wall conductance with pressure is small or nonexistent, suggesting that the wall region is dominated by conduction through the solid particle contact points or gas in the continuum regime.

5. A lower bound expression for the wall conductance of beds with high k_s/k_g ratios was presented. Based on this expression, for given values of k_s/k_g and k_{eff}/k_g, a conservative estimate of ratio of the bed thickness to particle size can be obtained as a function of desired values of bed-to-interface thermal resistances. For design application, this would help in choosing particle sizes and bed dimensions in order for the overall thermal behavior to be governed by the bed and not the interfaces and their associated uncertainties.

6. The thermal conductance at a beryllium-stainless steel cladding interface was analyzed based on the models of Lemczyk and Yovanovich and of Shlykov et al. Both models showed that the total conductance increases with decreasing roughness and with increasing P_c/H_{eff}. However, the differences in the prediction, particularly at higher values of P_c/H_{eff}, can be quite high, up to a factor of 3 for a roughness of ~1 μm. As a limiting case, assuming that contact always occurs, the desirable material roughness can be estimated based on maintaining the contact conductance as a small fraction of the total beryllium region conductance. For example, for a 3-cm beryllium region, assuming pure gas conductance within the roughness as a lower limit estimate of the contact conductance and assuming that the contact resistance must remain within 10% of the total region resistance, one obtains a maximum roughness value of the order of 10 μm.

7. The effect of beryllium block deflection occurring for thermal stress relief was assessed. The results indicate that beryllium block deflection can substantially reduce the interfacial conductance to an extent dependent on the size of the deflection, the contact pressure, and the roughness. For example, the total interfacial conductance can be reduced by up to 80% when the border deflection increases from 0 to 50 μm. Such effects can be accounted for in the design if properly characterized.

8. These observations indicate the importance of adequately predicting the contact conductance as a function of different parameters, such as the temperature, roughness, and contact pressure. The large variation between the predictions by the two models discussed earlier indicates that such characterization needs to be done experimentally using the prototypical materials for which an experimentally based model could then be developed for blanket analysis application.

VI.B. Conclusions from Assessment of Thermal Control Mechanisms

In light of these results, an assessment of the thermal control mechanisms applicable to ceramic breeder blanket designs was performed. The assessment was based on example calculations for ITER-like operating conditions. Although the absolute controllability of the ceramic breeder would change for different assumptions regarding the ceramic breeder material, power densities, and coolant type and temperature, it is believed that the comparative assessment of the different mechanisms would still apply. Four cases were considered: a helium gap, a sintered block beryllium region, a sintered block helium region with a metallic felt at the beryllium-cladding interface, and a beryllium packed-bed region.

A helium gap is attractive because of the simplicity of the design, and it provides for a reasonable wall load range, 0.55 to 2 MW/m^2 for the example case considered (excluding the effect of thermal radiation). However, the gap size required is small, ~1.5 mm in

this case, leading to the concern of maintaining close tolerances during manufacture and operation. Radiation can significantly increase the range of allowable wall loads up to a factor of ~2 depending on the emissivity of the surface. The calculations also indicate limited possibilities for active thermal control for the helium gap, particularly for lower coolant pressure cases.

Beryllium in sintered block form has a high thermal conductivity, which results in a thick beryllium layer. This tends to minimize the number of layers but can result in a large amount of beryllium, which is costly. The range of allowable wall load tends to be smaller than in the helium gap case because, in contrast to helium, the beryllium thermal conductivity decreases with temperature. For the example case, a beryllium region thickness of 5.3 cm provides an allowable wall load range of 1 to 2 MW/m^2.

Placing a felt at the beryllium-cladding interface provides the advantages of potentially better contact conductance predictability, accommodation of beryllium swelling and thermal expansion, and the possibility of active thermal control through gas pressure adjustment. For the example considered, for a felt thickness of 2 mm at the low-temperature beryllium-cladding interface, the allowable wall load range is 0.7 to 2 MW/m^2, and the beryllium sintered block thickness is reduced to 2.2 cm. Issues relate mainly to the performance of the felt in an irradiation environment.

Beryllium in packed-bed form offers the advantages of active control through gas pressure adjustment and minimum use of beryllium based on its lower thermal conductivity. However, this might lead to a higher number of layers in the design. For the binary packed bed considered, the ratio of k_{eff} at 1 atm to k_{eff} at 0.1 atm is ~2. This provides substantial additional flexibility for power variation accommodation through active thermal control. For the example case, a packed-bed thickness of 1 cm results in an allowable wall load range of 0.58 to 2 MW/m^2. For ITER test module application and for power reactor application, active thermal control is very appealing because of the increased flexibility provided in allowing for ceramic breeder blanket operation over a wide range of power levels. In addition, for ITER test module application, active control would allow for testing at different breeder temperature levels for a given power level.

NOMENCLATURE

A_{uc} = unit cell area

a = beryllium block dimension

d = diameter

E = Young's modulus

f = ratio of bed to interface thermal resistances

f_{max} = ratio of maximum to reference wall load

f_{min} = ratio of minimum to reference wall load

H_{eff} = effective material microhardness

h_w = packed-bed wall conductance

Kn = Knudsen number for a gap

k = thermal conductivity

k_{eff} = packed-bed effective thermal conductivity

k_w = effective thermal conductivity near wall

L = heated length of test section

L_0 = local distance between large particles of binary bed beyond which fine particles do not fit (see Fig. 13)

Nu = Nusselt number

P = pressure

P_c = contact pressure

P_N = neutron wall load

Pr = Prandtl number

Q = power to the heater

q = heat flow

q'' = heat flux

q''' = heat generation per unit volume

$(R_1/R_2)^2$ = fraction of interfacial area over which roughness occurs

Re = Reynolds number

r = radius

r_b = unit cell length of k_{eff} model

r_f = unit cell width for k_{eff} model

S_{ft} = ultimate tensile strength of material

T = temperature

T_{b1} = bulk temperature nearest to inner wall following bed temperature distribution

T_1 = temperature at lower boundary of unit cell

T_2 = temperature at upper boundary of unit cell

t_{gap} = nominal gap thickness

x_w = wall region thickness

Greek

α = thermal accommodation coefficient for gas

δ = thickness of thermal control region

δ_l = local characteristic length

δ_r = roughness

Δ_{max} = maximum bending deflection

ΔT = temperature difference

ΔT_{bed} = temperature difference across bed

ΔT_w = difference between wall temperature and packed-bed extrapolated temperature at the wall

$\Delta V/V$ = volumetric expansion of beryllium block

ϵ = porosity volume fraction

γ = ratio of specific heat at constant pressure to specific heat at constant volume for gas

λ = gas mean free path

υ = Poisson's ratio

θ = angular direction in cylindrical coordinate expression

σ = effective jump distance

Subscripts

(*ave*) = average

Be = beryllium

CB = ceramic breeder

c = contact

(*con*) = continuum regime

e = extrapolated

f = film

g = gas

He = helium

i = inner annular surface

o = outer annular surface

p = particle

r = roughness

s = solid

st = steel

std = standard

tot = total

uc = unit cell

w = wall

(0) = initial

(1) = final

ACKNOWLEDGMENTS

The authors would like to thank Parham Adnani, Zinovy Gorbis, Alice Ying, and Peter Huemer for their contributions to the effective thermal conductivity modeling, sintered block interface resistance analysis, felt calculations, and packed-bed experiment, respectively.

This work was performed under U.S. Department of Energy contract DE-FG03-88ER52150.

REFERENCES

1. "ITER Blanket, Shield and Materials Data Base," ITER Documentation Series No. 29, International Atomic Energy Agency (1991).

2. Y. GOHAR et al., "U.S. Technical Report for the ITER Blanket/Shield–A. Blanket," ITER-TN-BL-5-0-3, ITER Project (July–Nov. 1990).

3. M. A. ABDOU et al., "Blanket Comparison and Selection Study," ANL/FPP-83-1, Vol. II, Argonne National Laboratory (1983).

4. M. S. TILLACK et al., "Experimental Study of the Effective Thermal Conductivity of a Packed Bed as a Temperature Control Mechanism for ITER Ceramic Breeder Blanket Designs," presented at 13th Symp. Fusion Engineering, Knoxville, Tennessee, October 2–6, 1989.

5. M. S. TILLACK et al., "Experimental Studies of Active Temperature Control in Solid Breeder Blankets," *Fusion Eng. Des.*, **17**, 165 (1991).

6. R. BAUER and E. U. SCHLUNDER, "Effective Radial Thermal Conductivity of Packings in Gas Flow. Part II. Thermal Conductivity of the Packing Fraction Without Gas Flow," *Int. Chem. Eng.*, **18**, *2*, 189 (1978).

7. M. DALLE DONNE and G. SORDON, "Heat Transfer in Pebble Beds for Fusion Blankets," *Fusion Technol.*, **17**, 597 (1990).

8. D. KUNII and J. M. SMITH, "Heat Transfer Characteristics of Porous Rock," *AIChE J.*, **6**, 71 (1960).

9. R. O. A. HALL and D. G. MARTIN, "The Thermal Conductivity of Powder Beds. A Model, Some Measurements on UO_2 Vibro-Compacted Microspheres, and Their Correlation," *J. Nucl. Mater.*, **101**, 172 (1981).

10. P. ADNANI, A. R. RAFFRAY, M. A. ABDOU, and I. CATTON, "Modeling of Effective Thermal Conductivity for a Packed Bed," UCLA-FNT-29, University of California–Los Angeles (Nov. 1989).

11. A. R. RAFFRAY et al., "Model for Determining the Effective Thermal Conductivity of Particle Beds with High Solid-to-Gas Thermal Conductivity Ratio," presented at 13th Symp. Fusion Engineering, Knoxville, Tennessee, October 2–6, 1989.

12. M. J. ADES and K. I. PEDDICORD, "A Model for Effective Thermal Conductivity of Unrestructured Sphere-Pac Fuel," *Nucl. Sci. Eng.*, **81**, 540 (1982).

13. R. K. McGEARY, "Mechanical Packing of Spherical Particles," *J. Am. Ceram. Soc.*, **44**, *10*, 513 (1961).

14. A. ULLMAN, R. ACHARYA, and D. R. OLANDER, "Thermal Accommodation Coefficients of Inert Gasses on Stainless Steel and UO_2," *J. Nucl. Mater.*, **51**, 277 (1974).

15. D. R. OLANDER, "Fundamental Aspects of Nuclear Reactor Fuel Elements," TID-26711-P1, p. 137, Technical Information Center, Office of Public Affairs, Energy Research and Development Administration (1976).

16. J. TOBIS and D. ZIOLKOWSKI, "Modelling of Heat Transfer at the Wall of a Packed-Bed Apparatus," *Chem. Eng. Sci.*, **43**, *11*, 3031 (1988).

17. S. YAGI and D. KUNII, "Studies on Heat Transfer Near Wall Surface in Packed Beds," *AIChE J.*, **6**, *1*, 97 (1960).

18. S. YAGI and D. KUNII, "Studies on Heat Transfer in Packed Beds," *International Development in Heat Transfer*, Part IV, p. 750 (1962).

19. A. R. RAFFRAY, "Packed Bed Wall Conductance," UCLA-FNT-58, ENG-93-01, University of California–Los Angeles (July 1992).

20. Z. R. GORBIS, A. R. RAFFRAY, and M. A. ABDOU, "Study of Effective Solid-to-Solid Contact Thermal Resistance and Its Application to Solid Breeder Blanket Design for ITER," *Fusion Technol.*, **19**, 1519 (1991).

21. T. E. LEMCZYK and M. M. YOVANOVICH, "New Models and Methodology for Predicting Thermal Contact Resistance," *Heat Transfer Eng.*, **8**, 2 (1987).

22. Yu. L. SHLYKOV, "Calculating Thermal Contact Resistance of Machined Metal Surfaces," *Teploenergetika*, **12**, *10*, 79 (1965) (in Russian).

23. V. A. MALKOV et al., "Contact Heat Transfer in Gas Turbine Engines and Power Installations," *Mashtinostroenie* (1978) (in Russian).

24. M. S. BILLONE and S. MAJUMDAR, "Thermomechanical Analysis of the U.S. Solid Breeder Design," Argonne National Laboratory (Mar. 1990).

25. R. D. McCARTY, "Thermophysical Properties of Helium-4 from 2 to 1500 K with Pressures to 1000 Atmospheres," Technical Note, National Bureau of Standards (Nov. 1972).

26. R. K. SHAH and A. L. LONDON, *Laminar Flow Forced Convection in Ducts*, p. 153, Academic Press, New York (1978).

27. W. M. ROHSENOW and J. P. HARTNETT, Eds., *Handbook of Heat Transfer*, Chap. 7, McGraw-Hill, New York (1973).

28. M. C. BILLONE, S. MAJUMBAR, H. HASHIZUME, and A. R. RAFFRAY, "Thermal-Mechanical Analyses of the Be Multiplier Zones," Report of U.S. Contributions to the Homework for ITER (Feb./Mar. 1989).